UNIVERSITY OF TWENTE. | FRAUNHOFER INNOVATION PLATFORM
FOR ADVANCED MANUFACTURING

Department of Engineering Technology

Master's thesis (202000249)

Numerical investigation on the thermal behavior of li-ion batteries under various cooling methods

Mechanical Engineering: (Design and Manufacturing)

Abhay Patel s2767864
Committee chair UT : Prof. Dr. Ing. S. Thiede
Supervisor UT : Dr. Ing. S. Yang
Supervisor FIP: Beumkes Gijs
External Committee : Dr. S. Hajimolana
Date of Colloquium: 26th September 2023
Document Number: DPM2040

Enschede, September 19, 2023

Abstract

In this study, thermal management of the lithium-ion (Li-ion) battery pack for low-range applications such as E-bikes, electric scooters, solar equipment, etc. is contemplated. A major problem related to batteries operating at a high temperature which leads to thermal runaway has been studied. Various stages of the thermal runaway are discussed briefly. Safety issues associated with Li-ion batteries such as the causes that lead to thermal, mechanical, and electrical abuse, how they impact the battery structure and further lead to thermal runaway have been discussed in the study. The extreme working conditions and uneven distribution of the temperature, affect the effectiveness and the battery life, the focus of the study is to examinate the thermal behaviour of cylindrical Li-ion batteries and the optimization of the parameters to achieve a reduced temperature in the batteries and uniformity across the battery pack during the discharging operation. To ensure that the battery pack operates in the range of optimal working temperature of 15^oC to 40^oC delivering better performance with safety, thermal analysis is performed on the batteries.

A 52V 18Ah Li-ion battery pack is used and to simplify the computation and reduce its time, two modules of 4S1P are subjected to various cooling scenarios. The study uses Ansys - Computational Fluid Dynamics (CFD) to set the thermal model and execute the simulations under varied parameters like cell spacing, ambient temperatures, inlet velocities (in the case of forced convection), discharge rates, etc. The findings in the study depict that the temperature of the batteries is drastically reduced when natural convection and forced convection cooling are compared. After analyzing the cooling performance of the forced convection, cooling of the battery modules with the use of phase change materials (PCM) is investigated. The results show that the phase change material provides more uniformity in the temperature throughout the modules lowering the overall temperature of the battery pack.

Nomenclature

EV	Electric vehicle
BMS	Battery management system
C-Rates	Discharge Rates
HEV	Hybrid Electric Vehicles
Li-ion	Lithium Ion
3-D	Three Dimenisonal
2-D	Two Dimensional
PCM	Phase Change Material
4S1P	4 Series 1 Parallel
Pb	Lead-Acid
Ni-Cd	Nickel Cadmium
NiMH	Nickel Metal Hydride
SEI	Soli-Electrolyte Interface
NREL	National Renewable Energy Laboratory
BTMS	Battery Thermal Management System
CFD	Computational Fluid Dynamics
UAV	Unmanned Aerial Vehicles
SOC	State Of Charge
Re	Reynolds Number

Contents

1 Introduction

In the introductory chapter, an extensive overview is given of the objectives of this research, its importance, and why it is necessary. In the end, the scope of the thesis is discussed.

1.1 Research Objectives

The working temperature of the batteries plays a crucial part in establishing their reliability, longevity, and performance. All the parameters mentioned above are interlinked with the thermal performance [1]. The research in this area has given evidence that when there is an increase in the working temperature of the battery than the rated temperature range, it significantly affects the capacity of the battery, degrades the cell chemistry affects the nanostructure of the electrodes, and ultimately leads to shortened battery life. The objectives of this research work are as follows:

- To understand the influence of active and passive cooling on battery modules.
- Prevention of the battery cells from overheating and maintaining the optimal operating temperature is the primary objective of this research.
- To maintain the uniform temperature distribution across the battery modules.
- Analyzing the cooling efficiency of different methods such as natural convection, forced convection, and phase-change materials by varying the discharge rates (C-Rates).
- Simulating the cooling methods at different ambient temperatures with varying C-rates and distance between the batteries to find an effective way of cooling the batteries.

1.2 Importance Of The Research

The biggest challenges the world is currently facing are climate change, air pollution, reduction of fossil fuels, and controlling carbon emissions. Combining all the modes of transportation with its growing demand itself accounts for 49% of the world's fuel consumption through oil resources. To tackle this problem there is a major shift in renewable technologies replacing non-renewable technologies. Focusing on the transportation aspect and aligning the scope of the research work, Li-ion batteries are considered the most promising energy source to power hybrid electric vehicles [2]. Figure1 shows the prediction of Li-ion batteries demand in upcoming years.

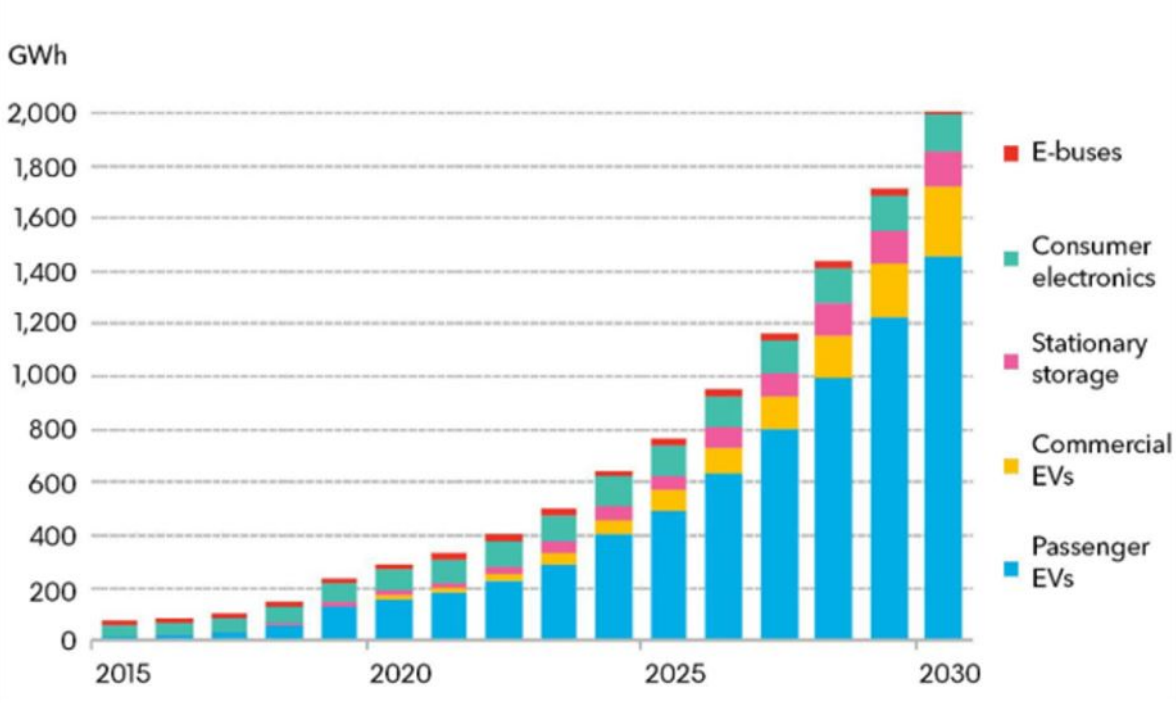

Figure 1: Demand of Li-ion batteries annually [3]

Recent trends in the demand for Li-ion batteries show a steep rise in their demand in various industries for high energy sources. There are certain issues that come along with the technology such as thermal runaway, internal short-circuits, reduced cycle life and environmental impact are few of them. Tracing various incidents concerning the safety of lithium battery operation has shown thermal failure as its major cause [4]. Thermal failure occurs when the temperature of the batteries keeps on increasing uncontrollably[5]. This may lead batteries to unwanted explosions or fires. Hence, this research focuses on improving the thermal management and problems associated with it, for the Li-ion battery pack for low-range applications.

Considering the low-range applications of the battery pack it is important to take into account the reliability, cost, and efficiency of the cooling methods. Based on these factors passive and semi-passive cooling methods seem to be viable as well as reliable options. In accordance with the latest advancements in the technologies for thermal management, 3-D simulations for natural convection, forced convection, and phase change material (PCM) cooling are performed and studied.

1.3 Research Scope

The objective of this thesis as discussed in the previous sections is to design and study efficient cooling systems for low-range EV applications. Cylindrical 21700 Li-ion batteries are considered. The scope of the research states that the base modules for the battery pack used are to be in 4S1P (4 series 1 parallel) configuration which is a (4x1) module. To simplify the geometry and reduce the computations a simple cylindrical geometry of the Li-ion battery is modeled in Solidworks. The simulation is performed on two modules in parallel. For calculations of the heat generation 52V 18Ah battery pack is considered. The entire battery pack will consist of 56 batteries with 14 (4x1) modules powering the load up to 932.4 Watts.

2 Literature Review

This chapter will cover the basics of the batteries, the working principle, different types of cell chemistries, types of cooling methods, and recent studies showing the parameters that influence the temperature and thermal behavior of the batteries.

2.1 Batteries

A battery is a group of two or more cells that produce voltage between the electrodes and discharge current. A cell is a fundamental unit of a battery that produces electrical energy via chemical reactions.

The batteries are categorized into:

- Primary Batteries
- Secondary Batteries

Primary batteries are not reusable due to their irreversible cell chemistry. The batteries that can be charged and used again by applying reverse voltage are secondary batteries [6]. Batteries with various cell chemistries that fall under this category are Lead-Acid (Pb), Nickel Cadmium (Ni-Cd), Nickel Metal Hydride(NiMH), and Lithium Ion (Li-ion).

2.1.1 Working Principle

A battery comprises four basic components: A Separator, an Anode (negative electrode), a Cathode (positive electrode), and an Electrolyte as shown in Figure 2. Conversion of the chemical energy stored inside a battery cell to electrical energy is the basic working principle of the batteries. Oxidation reaction takes place at the anode which leads to build up of electrons. The agglomeration of the electrons at the anode creates an electrical difference between both electrodes. In order to stabilize the system the electrons move to the cathode through an external circuit which can be seen in Figure 3. The reduction reaction takes place at the cathode. So, a reversible redox reaction takes place during the charging and discharging operation of the batteries[8].

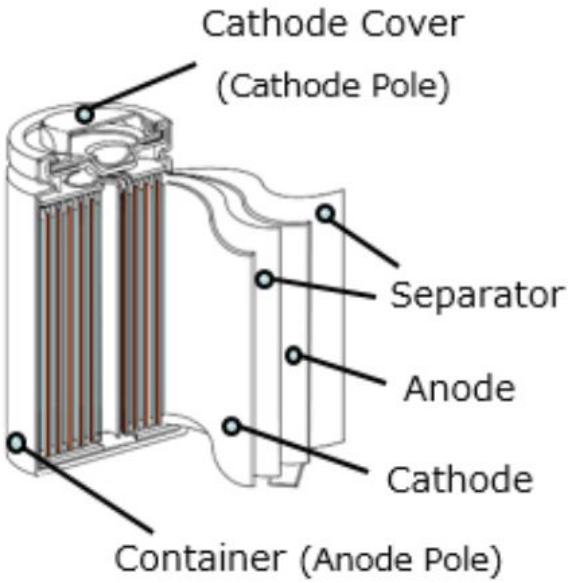

Figure 2: Battery components [7]

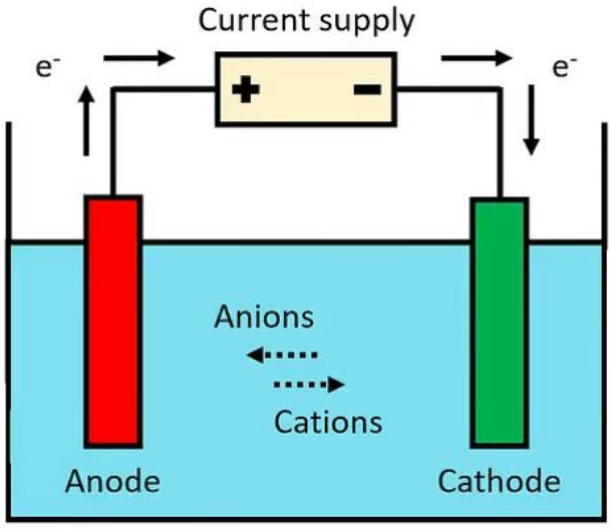

Figure 3: Diagram of battery cell during discharge[9]

2.1.2 Performance Metrics

Based on the application the batteries can be designed or adjusted to deliver low power for a longer duration of time or high power for short bursts. This burst of energy or current from the batteries depends on specific power and the duration of its delivery time depends on the battery's specific energy [10].

- Specific Power (W/Kg): It is the amount of power that a battery can deliver per kilogram.
- Power Density (W/m^3): The battery's capacity to deliver maximum available power per unit volume.
- Specific Energy (Wh/Kg): Amount of electrical energy stored per kilogram of the battery. Commonly known as gravimetric energy density.
- Energy Density (Wh/m^3): Amount of electrical energy stored per cubic meter of battery volume. Also, termed volumetric energy density.

To capture the performance characteristics of batteries with different cell chemistries Ragone plots are used. Ragone plots use specific power and specific energy as base parameters to compare different energy storage systems. As seen in Figure 4, the plot gives a visual representation of energy storage technologies that appear to be on the top right side and are considered to have better energy storage capacity and deliver energy quickly and efficiently.

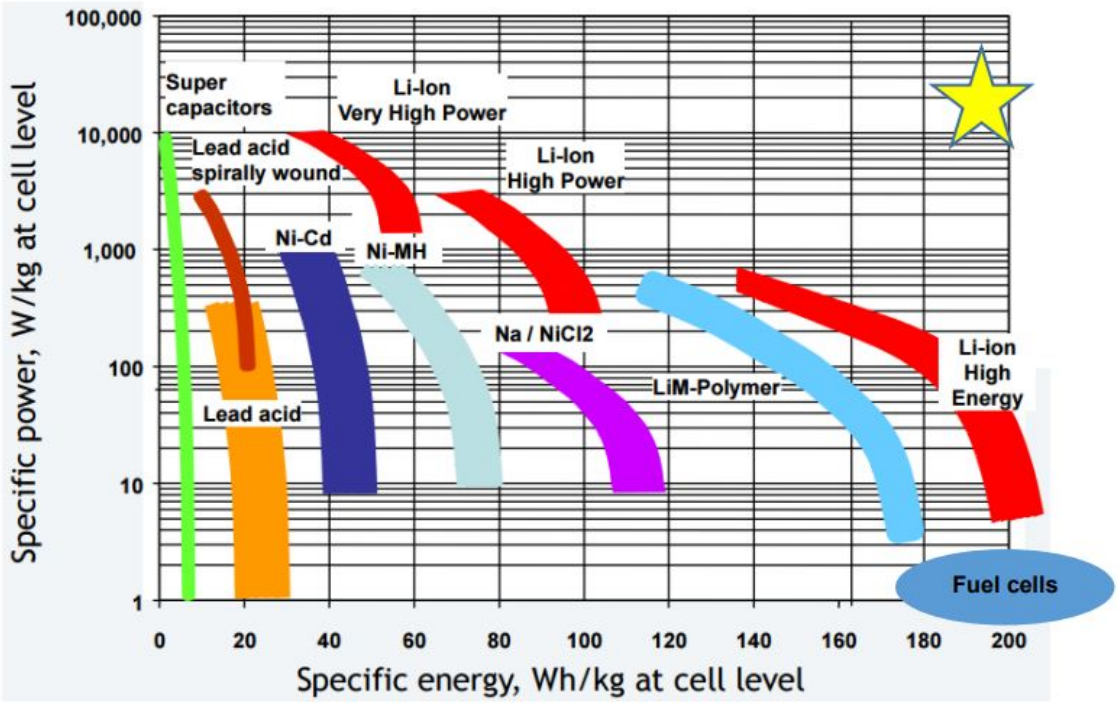

Figure 4: Ragone Plot[11]

	Li-ion	Lead-acid	NiCd	NiMH
Specific energy [Wh/kg]	100-300	30-50	45-80	60-120
Energy density [Wh/L]	125-600	50-90	50-70	160-420
Specific power [W/kg]	500-5000	50-180	100-150	100-500
Cycle life (to 80% of SoH)	2000-4000	500-800	300-1000	500-1000
C-rates [h^{-1}]	1-10	0.2	1	0.5
Operating temperature [°C]	-20 to 60	-20 to 60	-40 to 60	-20 to 60
Costs [€/kWh]	300-1000	100-200	300-600	300-600

Table 1: Characteristics of different types batteries [15]

2.2 Lithium-Ion Battery (Li-ion)

Lithium-ion batteries were developed around the 1970s and were commercialized by the 1990s [12]. During the discharge process, the battery uses positively charged lithium ions (Li+) to move from the anode to the cathode. Over other batteries, lithium metal has a significant advantage as it is the lightest of all metals and possesses the highest electrode potential. Also as observed in Table 1., compared to other batteries the Li-ion battery shows the highest energy density per kilogram having low maintenance with no memory effect (when a battery is recharged frequently when it is partially discharged the battery tends to lose its longevity) present. Degradation of the battery capacity is a common problem that comes along with aging in Li-ion batteries. The major problem that is related to the objective of this research is the possibility of thermal runaway of the battery[13][14]. Thermal runaway can be attributed to various reasons such as short-circuit, external heating, or formation of toxic gases.

2.3 Lithium-Ion Working Principle

The cathode and anode act as charge carriers responsible for the storage and release of the energy. The job of the separator is to prevent internal short circuits and allow the lithium ions (Li^+) to flow[16]. The electrolyte also carries lithium ions. Collective or individual failure of these components can raise safety concerns. Uncontrolled chemical reactions may lead to a significant amount of heat generation when a separator fails and in such cases, an electrolyte also acts as a fuel source to increase the heat generation rapidly[17][18].

The working of the basic Li-ion batteries is shown in Figure 5., Lithium ions are released from the cathode material (LiCoO2 for example), diffuse into the electrolyte, and pass through the nanopores of the separator to get inserted into the anode material during the charging operation [19]. The electrons migrate in the opposite direction from the external circuit to maintain the electro-neutrality. Lithium ions migrate from the anode toward the cathode during the discharging of the battery.

The reactions associated with charging and discharging [15]:

Cathode: $\mathrm{LiCoO_2} \rightleftharpoons \mathrm{Li_{(1-x)}CoO_2} + x\mathrm{Li}^+ + xe-$
Anode: $6\mathrm{c} + x\mathrm{Li}^+ + xe^- \rightleftharpoons \mathrm{Li}_x\mathrm{C}_6$
Reactions: $\mathrm{LiCoO_2} + 6\mathrm{C} \rightleftharpoons \mathrm{Li_{(1-x)}CoO_2} + \mathrm{Li}_x C_6$

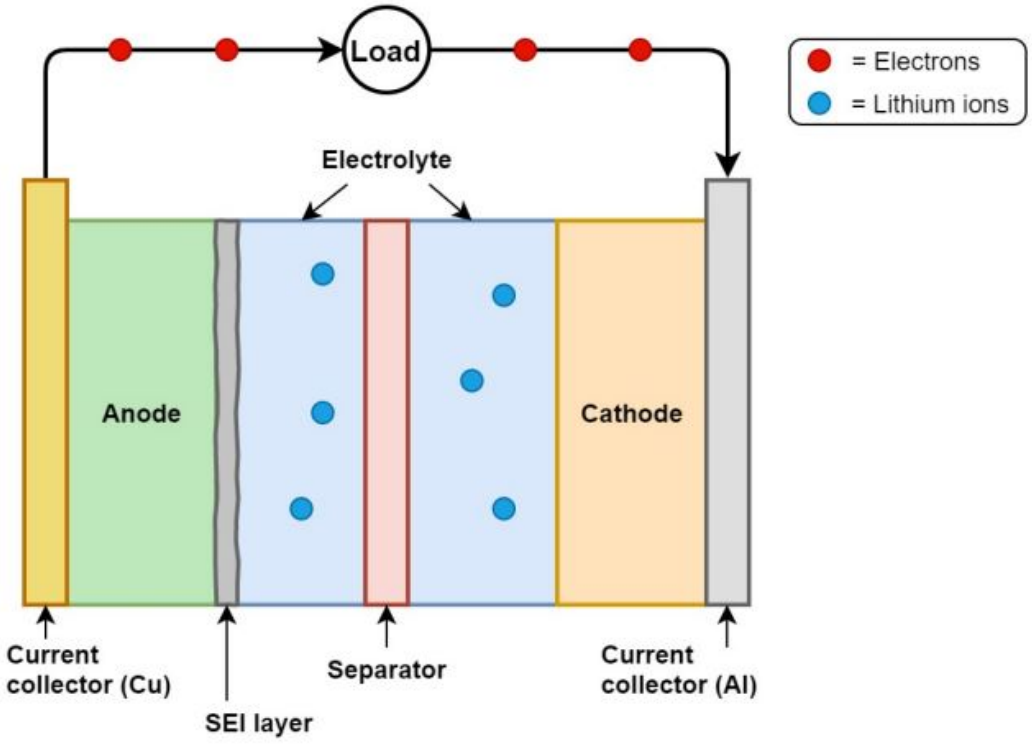

Figure 5: Representation of Li-ion battery during discharge [15]

2.4 Cell Geometry

The cylindrical cells are the most frequently used cell design. In this research, cylindrical Li-ion 21700 batteries are used as shown in Figure 6. Where 21 mm is the diameter and 70 mm is the length of the battery. Cylindrical batteries are cheap to manufacture and this geometry provides high structural strength. A battery cell and its working principle are already defined in the previous sections briefly. A battery module is formed when a fixed number of cells are combined in the casing to prevent any damage to the cells caused due to external shocks. And finally, the battery pack is composed of the modules and other components like BMS, its cooling system, etc. The complete flow of a cell to the module to pack is seen in Figure 6.

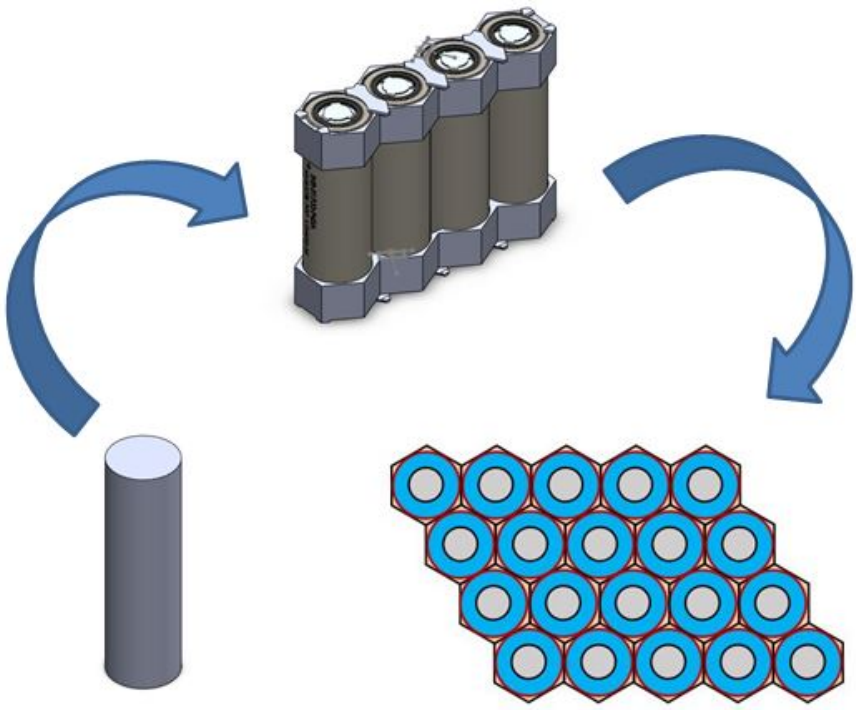

Figure 6: Making of battery pack starting from cell to form module and to form battery pack

2.5 Effect of extreme temperature conditions on the batteries

The role of a battery thermal management system comes in handy when the optimal working temperature of the batteries fails to stay in the operating temperature range of the application [20]. The optimal operating temperature range shown by various manufacturers in their datasheet(Li-ion) is between -20^oC to 60^oC as seen in Figure 7. Though various types of research and experimental data display the best performance delivered by the battery is when it manages to stay between the temperature range of 15^oC to 40^oC.

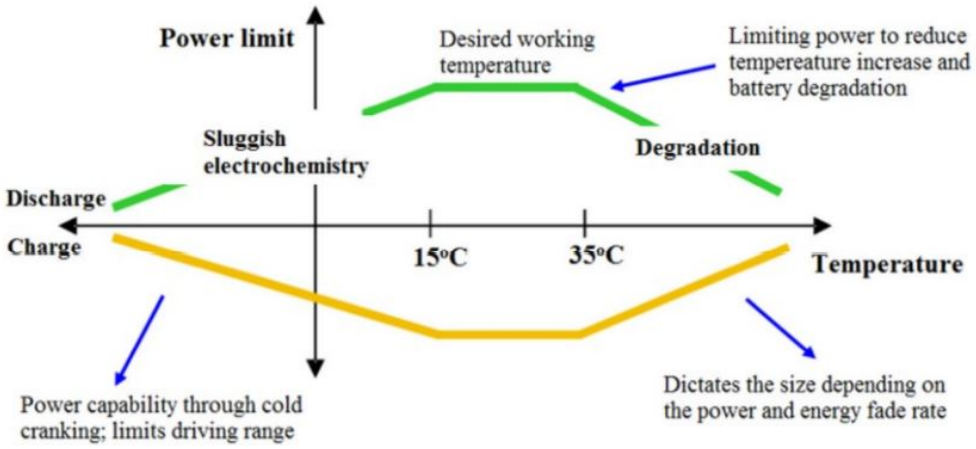

Figure 7: Operating temperature of Li-ion batteries[21]

The table 2 below shows the problems associated with the batteries during extreme ambient conditions.

Low Temperature (0^oC)	Capacity Drop Increase in the internal resistance
High Temperature (40^oC)	Decrease in the internal resistance Ageing phenomena accelerated Increase in self-discharge Leads to the decomposition of electrolytes Concerns regarding the thermal runaway and safety Reduction in the life cycle

Table 2: Impact of the extreme temperature conditions on batteries[22]

2.6 Failure modes in Li-ion batteries

Battery-generated heat cannot be completely extracted under normal operating conditions and this problem can have larger implications on a hot day or in a bigger battery pack. Figure 8. displays an overview of the safety issues for the batteries. Causes such as accidents, disasters, defects in cells, and poor system control contribute to mechanical, thermal, and electrical abuse. Further, these abuses affect parts of the batteries and can result in a thermal runaway (when a large amount of heat is generated indicating an exothermic reaction inside the cell, it is the onset of thermal runaway). When the temperature in the batteries rises the reaction rate inside the batteries also increases [23]. It is found that the reaction rate starts to increase from its self-generated heat when the battery reaches the temperature around 80^oC. This self-generation of heat and high temperatures with the cell chemical reaction leads to the formation of toxic gases and can potentially result in an explosion [24].

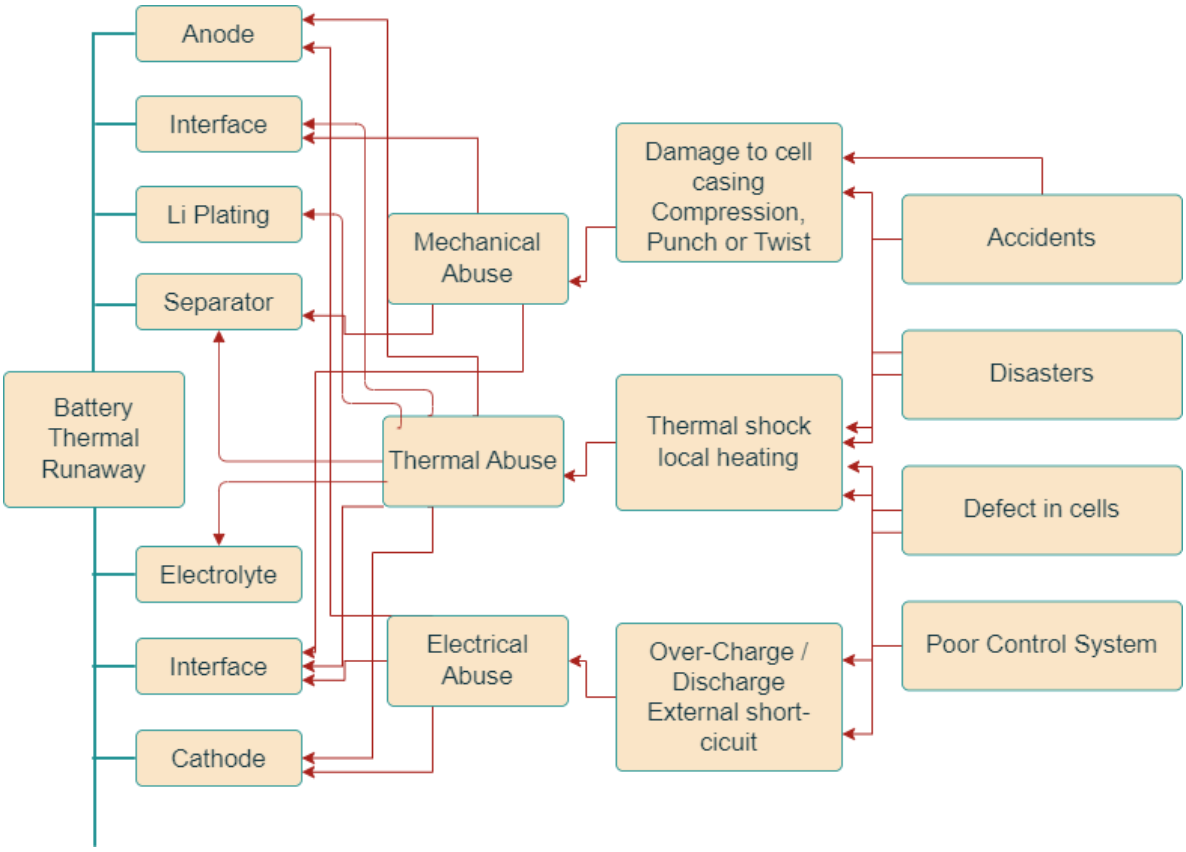

Figure 8: LIB safety issues [25]

2.7 Stages of Thermal Runaway

The thermal runaway temperature varies from cell size, design, chemistry, and materials used to manufacture battery components as seen in Table 2., Theoretically, there are four stages of thermal runaway; these stages are assigned based on the sequence of the components that are affected by the excessive heat produced during the process. It starts from the decomposition of the Solid-Electrolyte Interface (SEI), which leads to the reaction in the anode and electrolyte, then propagates to Separator Melting, and reaction between the cathode and electrolyte as described in the Figure 9. Different stages of thermal runaway can be seen in Figure 10, where the plot depicts the relationship between temperature rise and the cell temperature. The chart shows 3 stages of thermal runaway that is because stages 3 and 4 can occur simultaneously as well as together depending on the temperature condition of the batteries or self-heat generation rate [26] [27].

- Stage 1 (SEI Decomposition): It begins with the breaking of the solid-electrolyte interface (SEI), which initially emerges during the discharge process[28]. This

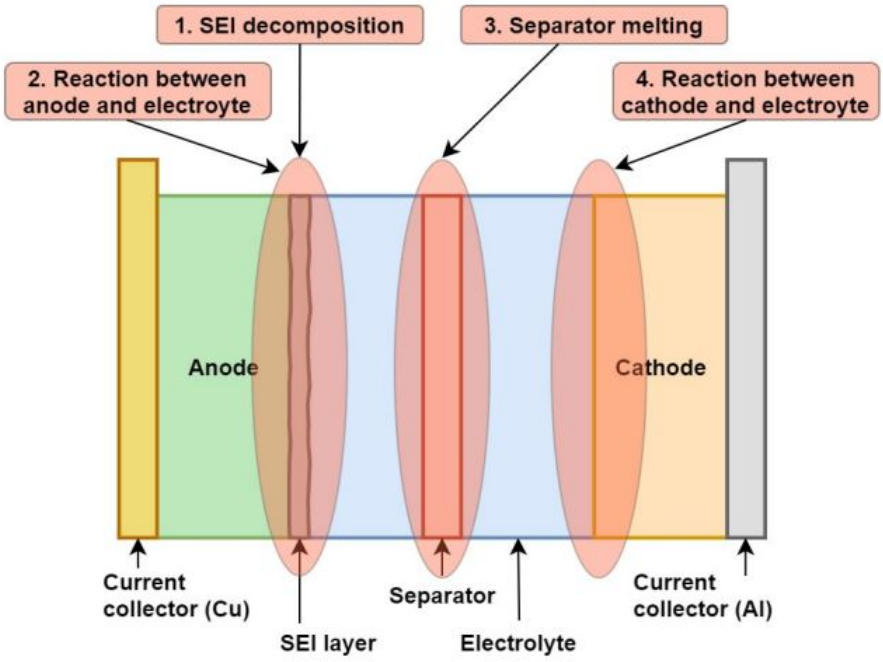

Figure 9: Thermal Runaway Stages [15]

interface blocks the electrons so that they do not decompose the electrolyte. The SEI decomposition roughly starts at 90^oC and the above temperatures. SEI partially decomposes being dysfunctional in forming the fence between the anode and the electrolyte [23].

- Stage 2 (Reaction between the anode and electrolyte): After the SEI layer is decomposed, eliminating the barrier between the anode and electrolyte. The reaction between the anode and electrolyte takes place at an elevated temperature between 100^oC and 120^oC. Temperature is even increased further when gases such as ethane and methane are released[29].

- Stage 3 (Melting of the separator): Polyethylene or Polypropylene is used as the separator material. The separator starts to melt around the temperature of 100^oC. During this stage shrinking of the separator is observed, which causes the cell to discharge by itself [28]. Over time, the anode and the cathode are exposed to each other, leading to an internal short-circuit [23].

- Stage 4 (Reaction between the cathode and electrolyte): This reaction can take place along with the melting of the separator at stage 3 [28]. 180^oC temperature is anticipated to be reached during this stage. Stages 3 and 4 together can be regarded as the stages where thermal runaway peaks as the increase in the tem-

perature and heat release rates are maximum [30].

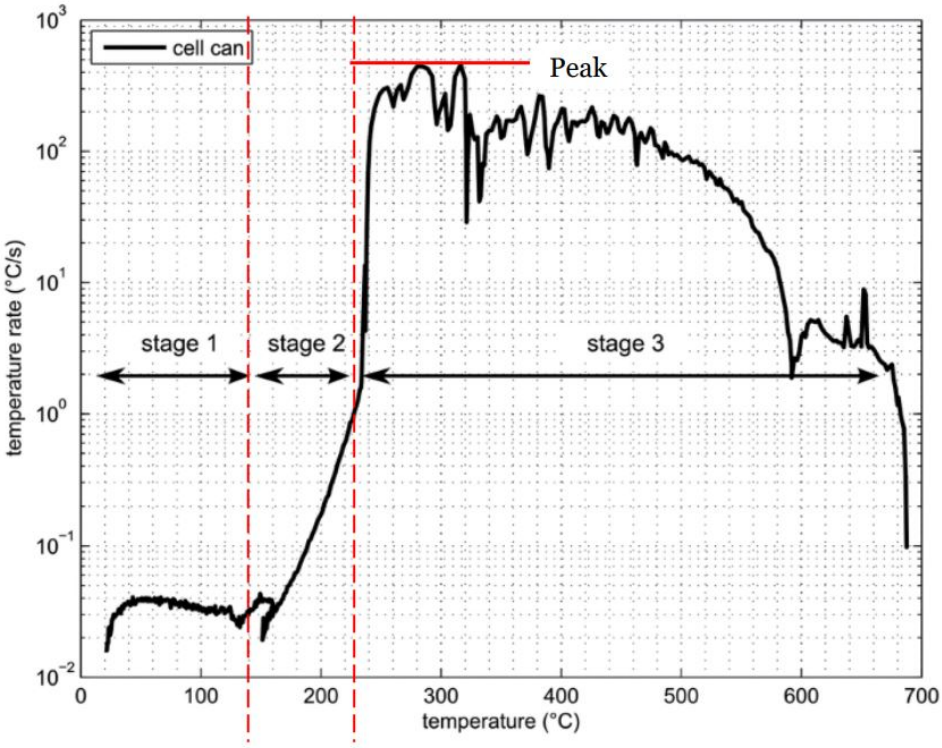

Figure 10: Thermal Runaway Plot: Rise in temperature rate vs Cell temperature [31]

2.8 Heat Generation

Based on the research carried out by the National Renewable Energy Laboratory (NREL) [32], indicate that there is a notable rise in the rate at which the heat is generated when cells are clustered within a battery module as shown in Figure 11. This is largely due to the densely packed structure which doesn't allow the air to pass through easily and lack of cooling capacity by the cooling medium. Hence, an investigation of two 4S1P (4x1) battery modules has been done in this research to understand the effect of heat generation and thermal behavior between adjacent cells.

Three heating strategies in the cell and amongst the cell have been studied by Ji et al. [33], by heating the lithium cells. The three strategies are:

- Self-Internal Heating: The internal resistance of the cells is higher at low temperatures, hence more heat is generated when the cells start discharging.
- Convective Heating: Convective method is the fastest way of heating. As the blower or fan is used to cool batteries, they themselves use the battery. Hot

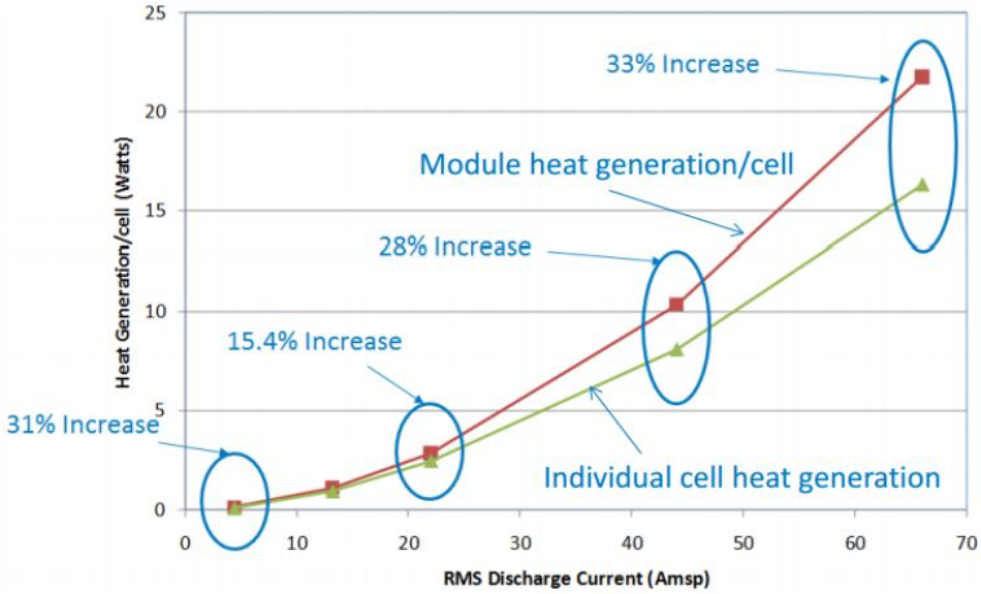

Figure 11: Deviation in heat generation rate in a module versus a single cell [32]

battery cells under the flow of air make the air around the battery warmer and the warmer air then passes to the surface of another cell and the air gets warmer and this carries on and eventually, cells are warmed by convective heat transfer.

- Mutual Pulse Heating: Programmed technique in the battery management system (BMS) to keep the battery pack within the best operational temperature range and ensure uniform temperature distribution throughout the battery pack by charging the discharged group of cells. This process between two groups of cells takes place simultaneously.

2.8.1 Thermodynamics in batteries

As discussed in the working principle section of the Li-ion batteries, the lithium ions are released from the cathode and get intercalated into the anode material. The thermodynamic potential difference between the cathode and anode determines the voltage of a cell. During the discharging of the cell, the quantity of the intercalated lithium ion in both the anode and cathode alters, resulting in the change in thermodynamic potential difference leading to modification in the cell voltage. The equation below shows the change in Gibbs free energy linked to the reaction at the cathode and anode. Where G stands for the Gibbs free energy, μ represents the electrochemical potential and S_i is denoted as the stoichiometric coefficient. In simple terms, it is the free energy of products minus reactants [34].

$$\Delta G = \left(\sum_i s_i \mu_i\right)_{\text{right}} - \left(\sum_i s_i \mu_i\right)_{\text{left}}$$

When no current flows in an electrochemical device, the system is considered to be in equilibrium. And the Gibbs free energy at the equilibrium can be related as

$$\Delta G = -nFU$$

U is denoted as the potential at which no current flows. A system in equilibrium still undergoes the reactions but the rate of both the forward and backward reactions are equal.

2.8.2 Heat Transfer

- Fourier's Law: Fourier's law asserts that the heat transfer rate across a material is directly proportional to the temperature gradient through the material and to the surface area, perpendicular to the gradient of the surface through which the heat passes. Mathematically it is represented as [34][35]

  $$Q = -k\nabla \mathrm{T}$$

  In this equation q represents the heat flux, k is the material's thermal conductivity of the material (W/mK), and ∇T stands for the temperature gradient in different dimensions. The One-dimensional heat transfer equation can be expressed as

  $$Q = -k\frac{dT}{dx}$$

- Heat Equation: The heat equation represents the alteration in a body's internal energy is directly proportional to the variation in the temperature of that particular body. Therefore, when the system reaches absolute zero temperature, there is no change in the energy, it can be mathematically expressed as

  $$Q = (C_p)\rho \mathrm{T}$$

  In the equation above C_p represents the specific heat capacity of the material (J/K) and ρ is the density in (Kg/m^3). Applying Fourier's law to the equation, the heat diffusion equation is obtained:

  $$\frac{\partial T}{\partial t} = \frac{k}{C_p\rho}\left(\frac{\partial^2 T}{\partial x^2} + \frac{\partial^2 T}{\partial y^2} + \frac{\partial^2 T}{\partial z^2}\right) + \frac{1}{C_p\rho}q$$

  q in the above equation is the internal heat generation

- Newton's law of cooling: It states that the change in the temperature or difference between the body and the surroundings is directly proportional to the rate of heat loss in a body, provided that the difference in the temperature is not significantly large. Mathematically represented as

$$\frac{dQ}{dt} = hA\Delta T$$

In the above equation, h is the heat transfer coefficient measured in (W/m^2K).

2.9 Cooling Methods

An appropriate battery thermal management system is required to maintain the battery's temperature in the ideal operating state. As discussed in previous sections about the adverse effects of thermal runaway, designing and efficient working of the BTMS should be the priority over factors such as weight, size, cost, and reliability.

2.9.1 Air Cooling

Cooling with the help of air is the most fundamental and traditional method for cooling. Due to its low cost and complexity, it is still in demand although it is not the most efficient method to cool because of air's low thermal conductivity and low heat capacity. Natural convection (passive cooling) and Forced convection (active cooling) are two modes of air cooling used. Natural convection is usually suitable for low-density batteries along with that to enhance the convection coefficient by using the blowers or fans. When it comes to cooling modules in the battery packs, due to their low heat capacity the overall system temperature rises significantly. Batteries near the inlet will have a relatively lower temperature than the batteries near the outlet. This leads to an uneven distribution of the temperature within the modules as well as the battery pack. In studies conducted by Wang et al.[36] best cooling performance is achieved when the position of the inlet or the fan is mounted on the top of the modules.

To cool the the battery packs having prismatic or pouch cells parallel cooling method is used. Cylindrical cells due to the complexity of integration of the plenum cannot adopt this cooling method. Figure 13. shows various types of manifold designs to improve cooling efficiency. The air is blown into the battery pack with the help of a fan or blower. To achieve uniformity of the temperature across the battery pack configuration of airflow rates, flow paths, positioning of inlet and outlet, spacing between the batteries, and layout of the batteries are necessary to be investigated. According to studies by Chen et al.[38] on the spacing between the batteries and its effect with several models of manifolds the objective was to decrease to the maximum temperature attained by the batteries and to obtain even temperature distribution throughout the battery pack. The major goal in the studies investigating the performance of air cooling is to improve the heat dissipation aligning with the design of the manifolds and orientation of the batteries. Numerous studies show the battery pack design in which

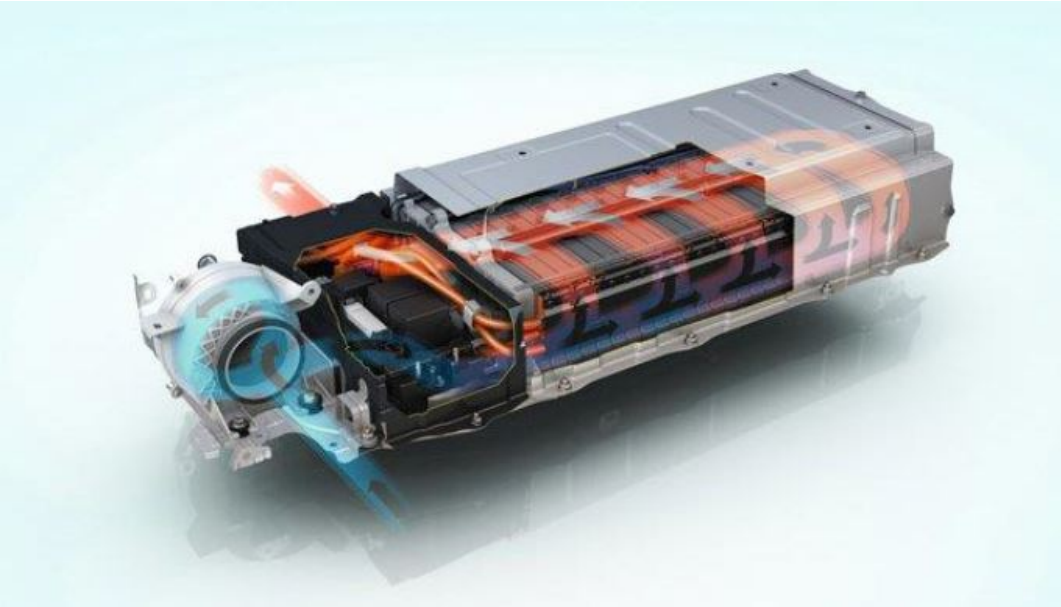

Figure 12: Air cooling used in Toyota Prius [37]

the airflow is horizontal is less efficient in terms of providing uniformity of the temperature when compared to the flow from a vertical or longitudinal direction. However, the tested channels do not help optimize the battery to safe operating temperature. U-type channel as seen in Figure 13 was suggested to overcome the issues observed in Z-type channels.

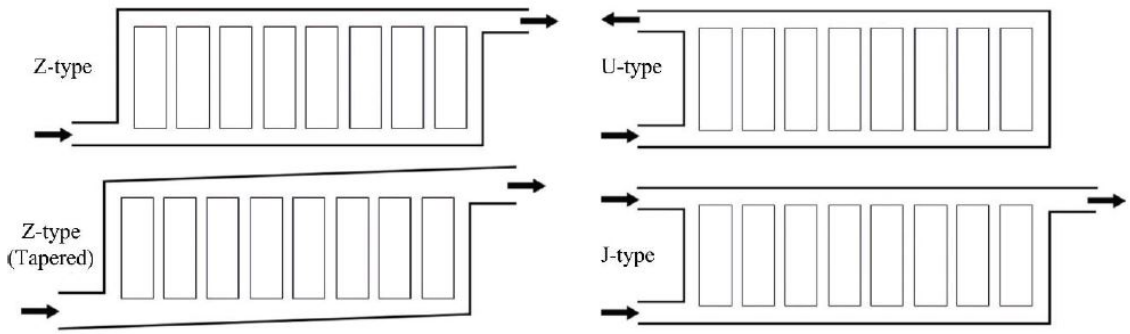

Figure 13: Different designs of manifolds used in BTMS [38]

2.9.2 Liquid Cooling

Liquid cooling outperforms air cooling as it has higher density and heat-carrying capacity. But liquid cooling also carries numerous drawbacks such as complexity, cost, and chance of coolant leakage. Cold plates are used in this liquid cooling method for prismatic and pouch-type cells. While the wavy serpentine channel is used to cool cylindrical batteries. In a study performed by Zhao et al.[39], they evaluated the performance of the wavy channel based on the parameters like velocity of the coolant at the inlet and at various C-rates. The findings indicated that if the coolant enters the wavy channel at 0.5 m/s having 25^oC as the inflow temperature at 5C discharge rate the maximum temperature within the pack rises to 35^oC and the temperature distribution across the battery pack can be kept under 1^oC.

A numerical analysis was conducted to investigate the influence of the direction of the coolant flow, the number of cooling channels, inlet dimensions, and mass flow rate on the thermal performance of the cooling method as depicted in Figure 14. The cooling method has coolant flowing through mini channels. The simulation results show that to keep the overall battery pack temperature below 40^oC, a minimum of 4 mini channels with the coolant inlet flow rate of 0.001 Kg/s are necessary [40].

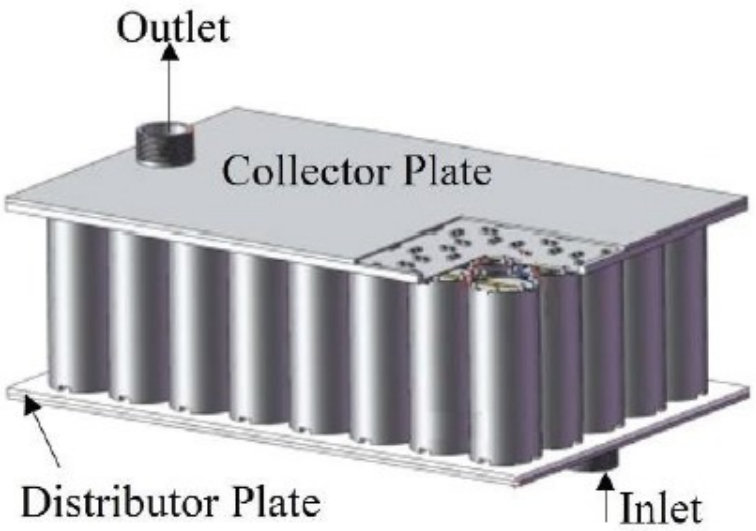

Figure 14: Liquid cooled cylinder by minichannels [40]

- Indirect Liquid Cooling: A lot of automobile manufacturers use the indirect mode

of liquid cooling. Manufacturers like Tesla, Chevrolet, Audi, etc. use this type of cooling method. They have cold plates running near the battery surface. These cooling plates contain small micro-channels that carry the coolant throughout the tubes as shown in Figure 15. Certain types of materials that are thermally conductive in nature but electrically isolating are used to separate the batteries and the cooling channels. To avoid any kind of potential short-circuits caused by potential coolant leakage, most of the connections are done outside the casing of the battery pack.

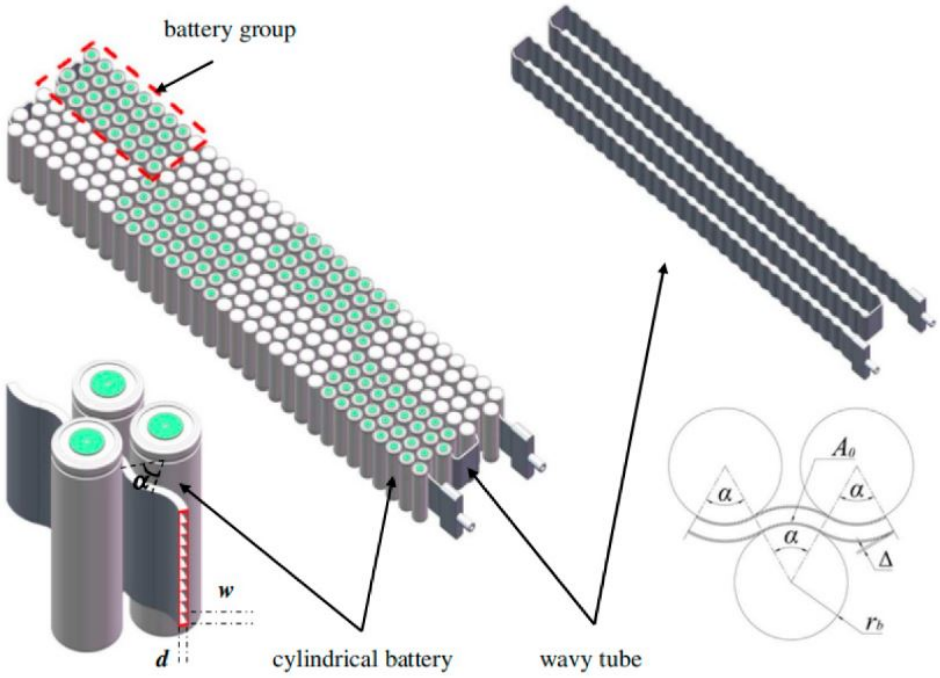

Figure 15: Wavy channels for liquid cooling [41]

- Direct Liquid Cooling: Direct liquid cooling is usually used by high-performance electric car manufacturer RIMAC. This technology has also been adapted by Koenisegg's Regera. Direct liquid cooling is also widely recognized as immersion cooling. It cools the battery pack uniformly and effectively as it covers the entire surface of the cell for cooling. Coolants possessing characteristics like less viscous along with a dielectric nature, high thermal conductivity, and high thermal capacity are suited for the operation. 3M (Minnesota Minning and Manufacturing Company) is a company that engineers coolants. One of the coolants they engineered has a boiling point around 76^oC, which helps batteries stay under optimal conditions even at high discharge rates.

Figure 16: Immersion cooling developed by Kreisel [42]

2.9.3 Phase Change Material(PCM) Cooling

Phase change materials are low-cost solutions for battery thermal management alternatives for passive cooling. A thermal management system with low operating cost, light in weight, and compact is considered to be an ideal battery thermal management system given that it maintains a safe operating temperature throughout the battery pack and across the modules. Al Hallaj and Selman [43], patented the technology and investigated the cooling efficiency of the battery packs comprising cylindrical Li-ion batteries (refer Figure 17.). Analyzing the results of the study they found out that by implementing the PCM battery life was extended when compared with ones without the PCM. The study also highlights that by using the PCM almost 90% of the battery capacity can be utilized from the battery pack. It has high latent heat and has the potential to cool the battery modules uniformly.

PCMs usually have their solidus and liquid temperatures in the range of battery operating conditions. This helps the battery to remain under optimal temperature conditions for a longer duration of time. Most commonly tested PCMs are paraffin often mixed with graphite to increase the thermal conductivity. Graphite flakes form a matrix which is useful when the paraffin melts at higher temperatures, the graphite matrix traps the paraffin and the composition retains its solid state. Every technology has its downside, if the batteries operate at high ambient temperatures for longer periods of time, the PCM will melt attaining its liquid state and reduced thermal conductivity and might even act as a thermal barrier.
The PCM's used to cool down the batteries and used in the BTMS should have the properties as stated below:

- High Latent Heat
- High Specific Heat
- Minimal sub-cooling (under extremely cold ambient conditions)
- Higher value of thermal conductivity
- Easy to avail and low in cost
- Chemically stable and non-toxic

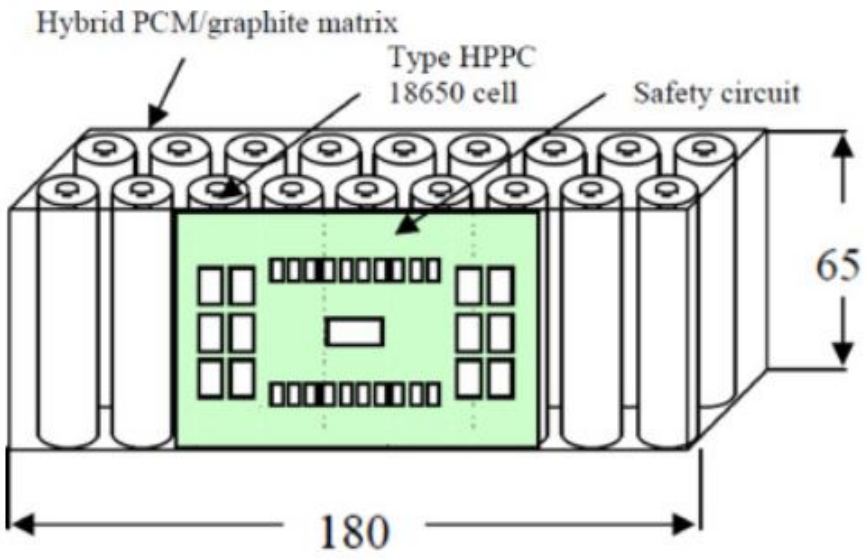

Figure 17: Represntation of PCM-Li-ion battery module

There are various classifications of the standard phase change materials. The phase change materials are basically categorized into:

- Solid-to-Solid PCMs (SSPCMs)
- Solid-to-Liquid PCMs (SLPCMs)
- Solid-to-Gas PCMs (SGPCMs)
- Liquid-to-Gas PCMs (LGPCMs)

Amongst the above-mentioned PCMs SLPCMs have a large latent heat capacity, and exhibit considerable stability during the phase change, and very small change in the volume is observed. Referring to Figure 18. it shows the bifurcation of the SLPCMs into organic, inorganic and eutectics. Table 3. displays the PCMs employed for the temperature range within 10^oC to 30^oC.

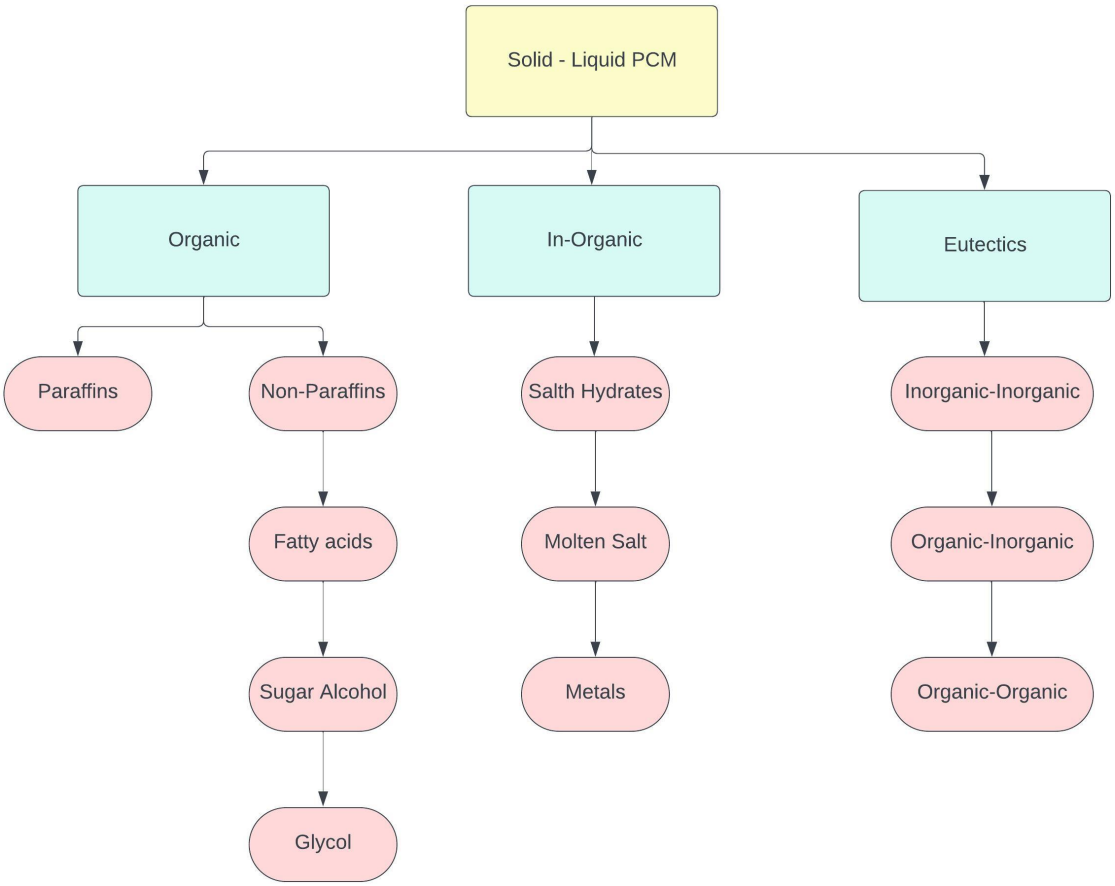

Figure 18: Categories of the phase change materials

As observed in the Table 4. Parrafin PCMs have a higher melting point than the PCM's operating in the temperature range 10^oC to 30^oC. This showcases that paraffins have a slight distinction between the two phases which is good for the PCMs as it helps in the storage of higher energy density in a compact volume. Paraffins are generated by the petrochemical industries. Hence, prices of the paraffins are market sensitive. For the application of cooling down battery packs slightly mushy phase of the PCM material and a small temperature difference for melting are desirable characteristics. Based on the optimal working temperature of the batteries PCMs having melting points below 40^oC are chosen for effective and uniform cooling.

Name	Melting Temperature	Latent heat of fusion (KJ/Kg)
Zinc Chloride	10	-
Pentadecane	10	205
Sulfuric Acid	10.4	100
Dipotassium phosphate	14	109
Propyl polmite	16-19	186
Dimethyl Sulfoxide	16.5	85.7
Hexadecane	16.7	237.1
Emerest 2325	17-21	138-140
Glycerol	17.9	198.7
Potassium Fluoride	18.5	231
Butyl Stearate	19	140
Propyl plamitate	19	186
Heptadecane	19	240
capric + Lauric	19.1	132
Polyethylene glycol	20-25	146
Iron bromide	21	105
Dimethyl Sebacate	21	120-135
Octadecyl 3-mencaptopropylate	21	143

Table 3: PCMs used for temperature range 10^oC to 30^oC [44]

Material	Melting Temperature (^oC)	Latent heat of fusion (KJ/Kg)	Thermal Conductivity (W/mK)
5913 (n-paraffin)	23	189	0.21
6106 (n-paraffin)	43	189	0.21
P116 (n-paraffin)	41	210	0.21
5838 (n-paraffin)	49	189	0.21
6035 (iso-paraffin)	59	189	0.21
6403 (iso-paraffin)	63	189	0.21
6499 (iso-paraffin)	67	189	0.21
Hexadecane	18	236	0.21
Heptadecane	22	213	0.21
Octadecane	28	244	0.21
Nonadecane	32	222	0.21
Paraffin Wax	55	146	0.21

Table 4: Organic Paraffin waxes as PCMs [44]

2.10 Comparative study of thermal management systems

Based on the discussion in the previous subsection about various types of thermal management systems, a comparative list of advantages and disadvantages is drawn out as seen in Table 5.

Cooling Method	Advantages	Disadvantages
Natural Convection	Low in cost	Poor thermal performance due to low heat transfer coefficient
	Almost zero operational cost	Ambient air temperature dependent
	Can be integrated easily	Reduction in maximum temperature limited
	Cooled passively	Limited effectiveness
Air forced Convection	Straightforward functionality	Low heat transfer coefficient
	Economical in terms of initial cost	Ambient air temperature dependent
	Requires low maintenance	Electricity drawn by fans
		Less uniformity in the temperature
		Limited effectiveness
Liquid Passive Cooling	Economical in initial cost	Risks of fluid spillage
	Low operational cost	Risk of loss of the gas
	Passively cooled	Inadequate in severe conditions
	Low maintainability	
Liquid Active Cooling	Enhanced heat transfer	Costly in setting up initial cost
	Increased uniform and even temperature distribution	Increased operational cost
		Complex functionality
		Risks of fluid spillage
		Reduced lifespan
		Electricity drawn by pumps
PCM	Low in cost	Comparatively less conductive
	Low maintainability	Risk of spillage
	Passively cooled	Regeneration of the phase change material
	Highly efficient	Potential for temperature dropping below the freezing point
	Increased uniformity and even temperature distribution	Difference in the volume with phase change

Table 5: Comparison of the thermal management systems [45]

3 Battery Thermal Characterization and Modeling

In this study, suitable BTMS is to be investigated for a 52V 18Ah battery pack for low-range applications such as E-bike, electric scooters, Unmanned Aerial Vehicles (UAVs), etc. It can be seen from Figure 19., the approach to modeling the 3-Dimensional computational fluid dynamics (CFD) thermal model. The battery module is modeled in Solidworks software. To understand and study the effect of heat generation from a cell with adjacent cells and modules closely, a part of the 56 cells 14S4P (14 x 4). Two modules of 4S1P are investigated with natural convection, forced convection, and PCM cooling techniques. 21700 Li-ion cell having 3.7 V and 4500 mAh is used in the battery pack. Table 6. displays the cell characteristics. The thermal CFD simulation is set up using ANSYS Fluent. The parameters varied to study the change in temperature and thermal behaviour of the cells are discharge rates (C-rates), inlet velocity during the forced convection setup, cell spacing, and variation in the ambient temperatures.

Assumptions for battery thermal model:

- Simplified Geometry: A simple cylindrical cell is modeled to reduce the computational complications.
- Radiation of the heat from the surfaces of the battery modules has been neglected.
- An Equal amount of heat generation is assumed through all the cells during the discharge.
- To reduce the computational time considerably for a large number of simulations laminar flow is assumed for forced convection setup.

Calculation of the Reynold's number:

At 2 m/s velocity, the fluid domain length is 0.04 m

$$Re = \frac{\rho u L}{\mu}$$

Density (ρ) = 1.225 Kg/$(m)^3$ and the dynamic viscosity (μ) = 1.7894 x $(10)^{-5}$ Kg/m.s

Substituting in all the values, the calculated Reynold's number is 54,501. Which is far away from the laminar region. As the forced convection simulation is just being performed on two modules and not on the entire battery pack, the deviation in the results is expected to be small. Nonetheless, one of the models for the forced convection simulation is simulated again by using the turbulent model to check the deviation in the results.

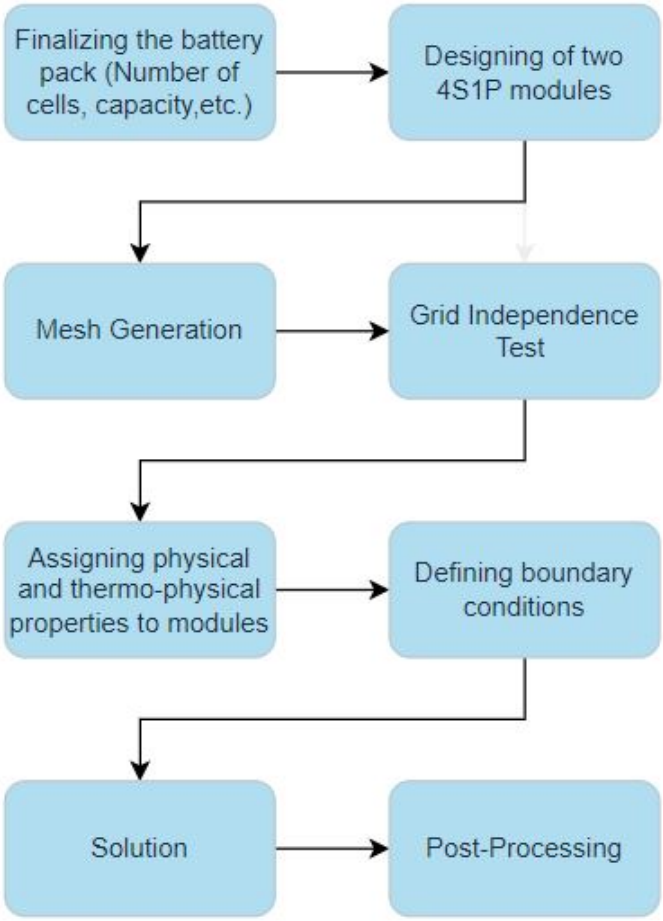

Figure 19: Methodology for the CFD Analysis

3.1 Selection of the thermal model

Going through several thermal models such as the lumped capacitance model, Equivalent circuit thermal models, and the Numerical and Analytical thermal models. The lumped capacitance thermal model uses the temperature of the body as the function of time meaning the temperature is assumed to be spatially independent. The equivalent circuit model uses the electrochemical and the mathematical model combining the voltage source, resistors, and capacitors to represent the physical structure of electrical circuits and systems[47]. The analytical and numerical methods encompass various approaches to address the complex heat transfer problem using the finite element method (FEM), finite volume method (FVM), finite difference method (FDM), and the boundary element method [37]. All the mentioned numerical methods may differ numerically and possess their own advantages and disadvantages as observed in Table 7.In compar-

Capacity	Typical	4500 mAh
		16.2 Wh
	Minimum	4300 mAh
		15.5 Wh
Cell Voltage	Nominal	3.6V
	Charge	4.2 V
	Discharge	2.5 V
Charge Current	Standard	4.5 A
	Maximum	13.5 A (70^oC cutt-off)
Charge Time	Standard	1.5 hr
Discharge Current	Continuous	45 A (70^oC cutt-off)
Temperature	Charge	0^oC to 60^oC
	Discharge	-40^oC to 60^oC
Energy Density	Volumetric	643 Wh/l
	Gravimetric	242 Wh/Kg
Typical Impedance	AC (30% SOC)	7 mΩ
	DC (50% SOC)	15 mΩ

Table 6: Cell Characteristics [46]

ison to other models, some of the models have the potential to produce precise results by solely accounting for Ohmic heating and entropic heating or cooling as the origin of the heat generation. When the lumped capacitance model and equivalent circuit model are taken into account they can produce accurate results for the computation of larger systems or entire battery packs saving a lot of time. Compared to other models numerical methods possess the advantage of visual representation of the results. If the thermophysical properties and the boundary conditions are set up well, the method produces very accurate results. Numerical methods are generally used by designers as they assist them nicely in improving the design and visualization of various aspects of the thermal management system.

Method	Advantages	Disadvantages	Recommended Application
Lumped Capacitance Model	One significant benefit of the model is it is simple to use with less data to be fed for an acceptable result. Quick and faster in design as the method lumps the characteristics neglecting the differences that are very small or which don't affect the results. It can also be coupled with other models like the equivalent circuit model and a few numerical models to simplify complex problems.	Physical constraints associated with various applications due to Biot number (Bi) limitation. Only be used for the application for Bi < 1. Inaccuracy was observed in the results for higher discharge rates and extreme operating conditions.	System-level modeling where fast processing time is required. Can be used for parameters involving no-extreme operating conditions.
Numerical and Analytical Thermal Models	Are not very complex and can yield very good accuracy in results. Enhancing the computational accuracy requires inputting the boundary conditions and thermo-physical properties at the expense of computation time.	Requires exact data of the material properties, chemical composition, and the physical representation of the energy storage system. The method is computationally intensive depending on the 2D or 3D model. Inflexible as the model can only be applied to a similar geometry or battery type.	Applications where a high degree of accuracy is required. Ideal for energy storage systems with cell-level modeling. Ideal tool when thermophysical properties are known. Very useful for system design optimization.

Equivalent Circuit Thermal Model	In comparison to other models they are swifter, more adaptable, and simpler to formulate. Feeding the data about the thermo-physical properties is minimal.	Similar to the lumped capacitance model as the model can only calculate the average temperature of the entire battery pack being less accurate.	System level modeling and fast modeling time required. Can be used with electrothermal modeling where electrical behaviour modeling is of significance.

Table 7: Different thermal models

From the above discussion Numerical and Analytical Thermal Model (CFD) Finite Volume Method, was chosen to perform the simulation as the goal of the simulation is to optimize the cooling and modify the parameters that affect it.

3.2 Calculations for 52V 18Ah battery pack

The power or load is derived from the batteries in series and in parallel. In this case, 14 batteries will be in series, and 4 sets of these 14 batteries in parallel would make 14S4P configuration of the battery pack.

Power(Load) = 932.4W

Current from the battery pack at 1C discharge rate (I_b)- 18 A

Similarly, current discharge at other C-rates will be calculated;

C-rate x (I_b)

At 0.5 C

0.5 x 18 = 9 A

At, 1C => 18 A

At, 1.5C => 27 A

At, 2C => 36 A

Heat Generation, Q(W)= $(I_c)^2$x(I_b)x internal resistance

Where (I_c) is the current of a cell at various discharge rates, (I_b) is the current of the battery pack and the internal resistance = $(10)^{-3}\Omega$

Q at 0.5C

Q = ((0.5)x(4.5))^2 x 18 x $(10)^{-3}$

Q = 0.091125 W

1C	0.3645 W
1.5C	0.820 W
2C	1.458 W

Table 8: C-rate and corresponding Power

As, per the geometry of the cell (simplified cylinder),

Volume of the cell = Π x $(r)^2$ x h

Volume = Π x $(0.021)^2$ x (0.070)

Volume = 0.0000969 m^3

In the fluent model when assigning the boundary condition the energy density in (W/$(m)^3$) is used as the heat generation rate per cell.

The, Energy density (W/$(m)^3$) = Heat Generated per cell /Volume of the cell

So, at 0.5C

Heat generation rate = 0.091125/0.0000969

Heat generation rate = 940.402 (W/$(m)^3$)

As we are computing for two 4S1P batteries so, 8 batteries in total generate heat;

Discharge Rate	Q single cell (W/m^3)	Q two modules (W/m^3)
1C	3761.609	30092.609
1.5C	8462.33	67698.33
2C	15046	120371

Table 9: C-rate and Heat generation with single cell and two modules

3.3 CAD Model

The simplified cylindrical geometry was modeled in Solidworks as seen in Figure 20. The 21700 battery's geometrical dimensions are, a diameter of 21 mm, and the battery height is 70 mm. In this study, cell spacing in the geometries has been modified to understand if the spacing between the cells impacts the overall cooling performance. The cell spacings varied in the geometries are 2 mm, 4 mm, and 6mm. These spacings are equally varied between the cells in series and in parallel (refer to Figure 21.) showing the top and side views of the modules.

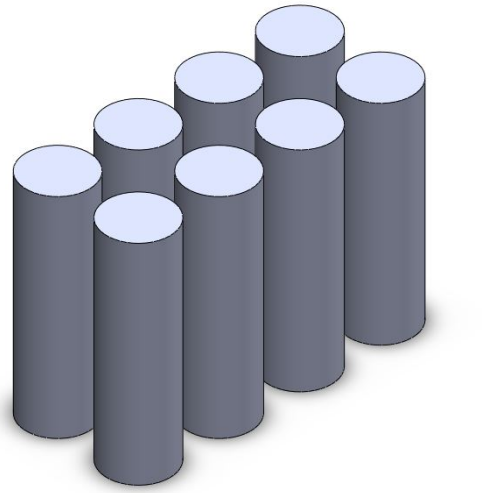

Figure 20: CAD model of 4S2P configuration

3.4 Governing Equations

Throughout the study, three simulation models are set up for the investigation of the temperature. Two modes of heat transfer are used; Convection and Conduction. Most of the forced convection simulations are performed by assuming laminar flow. But as discussed at the start of the section. Reynold's number calculated for the flow regime falls under turbulent flow. So, the model that shows better cooling performance for forced convection will go through the turbulent model to observe the deviation in the temperature values. So, for turbulent modeling, the K-epsilon-SST option has been used.

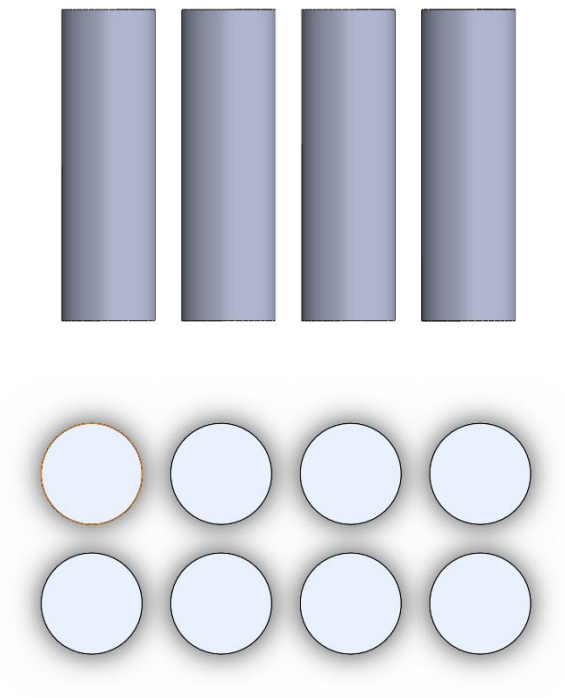

Figure 21: Side and top view of 4S2P configuration

3.4.1 Navier-Stokes Equation

Navier-Stokes equation is based on the principle of conservation of mass, momentum, and energy. It is the representation of these principles in the form of partial differential equations. Three fundamental principles are:

- Mass is Conserved: Mass of the flow stays constant with the time in a controlled volume. It can be expressed as:

$$\frac{\partial \rho}{\partial t} + \nabla \cdot (\rho \vec{V}) = 0$$

- Energy is Conserved: The total sum of work done and the heat added to the system combine to form the total energy of the system. It is expressed as:

$$\rho \left[\frac{\partial h}{\partial t} + \nabla \cdot (h \vec{V}) \right] = -\frac{Dp}{Dt} + \nabla \cdot (k \nabla T) + \phi$$

h is the enthalpy, ϕ shows the dissipation, and k is the thermal conductivity

From the left-hand side (LHS) of the equation, the two terms added show energy changes with time along with the convection term, and the remaining three terms on the right-hand side (RHS) of the equation represent the pressure work, diffusion term, and the dissipation term.

- F = ma (Newton's 2nd law of motion): The second law of motion asserts that the rate of change of momentum is equal to the direction and magnitude of the sum of forces applied to the system.

$$\frac{\partial}{\partial t}(\rho\vec{V}) + \nabla \cdot (\rho\vec{V} \otimes \vec{V}) = -\nabla p + \nabla \cdot \bar{\bar{\tau}} + \rho\vec{f}$$

Here, the viscous stress is denoted by T and f represents force per unit mass

3.4.2 Thermal Conduction

The diffusion of the thermal energy in the form of heat transferred from the body at a higher temperature to a body at a lower temperature when in contact. The 3D transient energy equation governing the thermal conduction in cylindrical cells can be represented as:

$$\frac{\partial}{\partial \mathrm{x}}\left(\frac{\partial \mathrm{T}}{\partial \mathrm{x}}\right) + \frac{\partial}{\partial \mathrm{y}}\left(\frac{\partial \mathrm{T}}{\partial \mathrm{y}}\right) + \frac{\partial}{\partial \mathrm{z}}\left(\frac{\partial \mathrm{T}}{\partial \mathrm{z}}\right) = \frac{\rho c_{\mathrm{p}}}{\mathrm{k}}\frac{\partial \mathrm{T}}{\partial \mathrm{t}}$$

The thermal conductivity of the cells depends from geometry to geometry. In this study, cylindrical-orthotropic thermal conductivity is selected. The radial thermal conductivity is 0.2 (W/mK) and the axial thermal conductivity is 37.6 (W/mK).

3.4.3 Convection

Natural convection is a buoyancy-driven process resulting in the convection from the bodies at higher temperatures. Gravitational force plays a major role in modeling natural convection along with the temperature-dependent density of the air. This develops convective flow caused by the difference in temperature between the surfaces.

$$\frac{\partial \rho}{\partial t} + \nabla \cdot (\rho \mathbf{V}) = 0$$

$$\rho\left(\frac{\partial \mathbf{V}}{\partial \mathrm{t}} + (\mathbf{V} \cdot \nabla \mathbf{V})\right) = -\nabla \cdot \mathrm{p} + \mu\nabla^2\mathbf{V} + \rho\mathbf{g}\beta\left(\mathrm{T} - \mathrm{T}_\infty\right)$$

$$\frac{\partial \mathrm{T}}{\partial \mathrm{t}} + \mathbf{V} \cdot \nabla \mathrm{T} = \alpha\nabla^2\ \mathrm{T}$$

3.5 Grid Independence test

Grid independence test is performed to assess the computational efficiency of the and to save time to achieve accuracy in results as much as possible. From Table 10. below it is observed that the average battery temperature of the modules was checked 8 times for different numbers of elements and nodes by refining the element size. Observing the trend of the results of average temperature in Figure 22., from the lowest number of elements (124447) to the highest number of elements (480175) a small variation in the value of average temperature was observed. From the metrics observed in this study mesh size with 125273 elements seems to give near-accurate results without costing a lot of computational time.

	No.of nodes	No. of elements	Avg. Temp	Body sizing (element size)	Face sizing (element size)
1	30715	124447	40.166919	0.005 m	0.008 m
2	31016	125273	39.7	0.008 m	0.1 m
3	36547	157173	39.825631	default	default
4	44017	171651	40.11874	0.001 m	0.005 m
5	49392	199030	39.92826	0.001 m	0.004 m
6	62068	264760	39.700327	0.001 m	0.003 m
7	76088	337788	39.230244	0.001 m	0.0025 m
8	102998	480175	39.17313	0.001 m	0.002 m

Table 10: Various number of elements to test grid independency

3.6 Boundary Conditions

For the forced cooling of battery modules with cell spacing (2mm, 4mm, and 6 mm) inlet velocities of 1 m/s and 2m/s are used. 3 m/s of velocity was used for the forced convection simulation modules with 2 mm of cell spacing. The inflow and the outflow for forced convection can be seen in Figure 23. The fluid and material properties used in the forced convection simulation can be seen in Table 11. Cylindrical Orthotropic thermal conductivity is assigned to the cell geometry for all simulation methods. Ambient temperature is varied to see its effects on the cooling performance. 0^oC, 24^oC, and 35^oC are the ambient temperatures varied for all the types of cooling methods. Lastly,

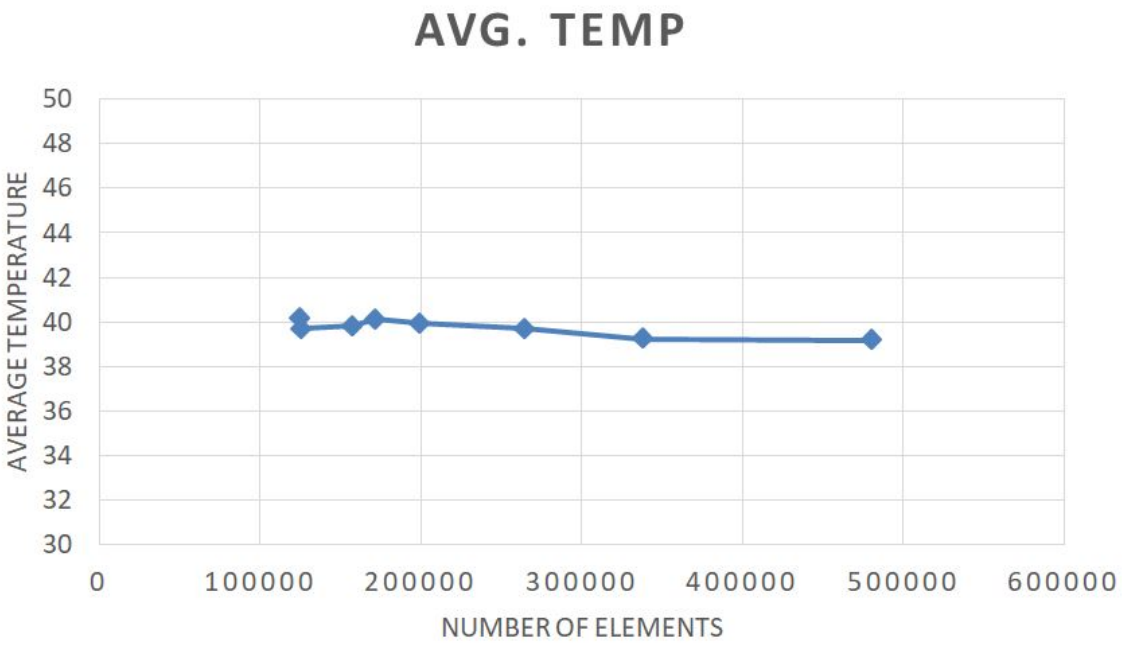

Figure 22: Grid Independence Test Results

the heat generations are varied for different discharge rates (1C, 1.5C, and 2C).

	Battery	Aluminium	Air
Density (Kg/m^3)	2268	2719	1.225
Heat capacity (J/Kg.K)	933.7	871	1006.4
Thermal Conductivity (W/m.K)	radial direction - 0.2 axial direction - 37.6	202.4	0.0242
Viscosity	-	-	0.000017894

Table 11: Thermo-physical properties

A similar configuration is set for the Natural convection cooling. Natural convection just does not have an inflow of air through external sources such as a fan or a blower. However, to stabilize the airflow in natural convection very small velocity of 0.001 m/s

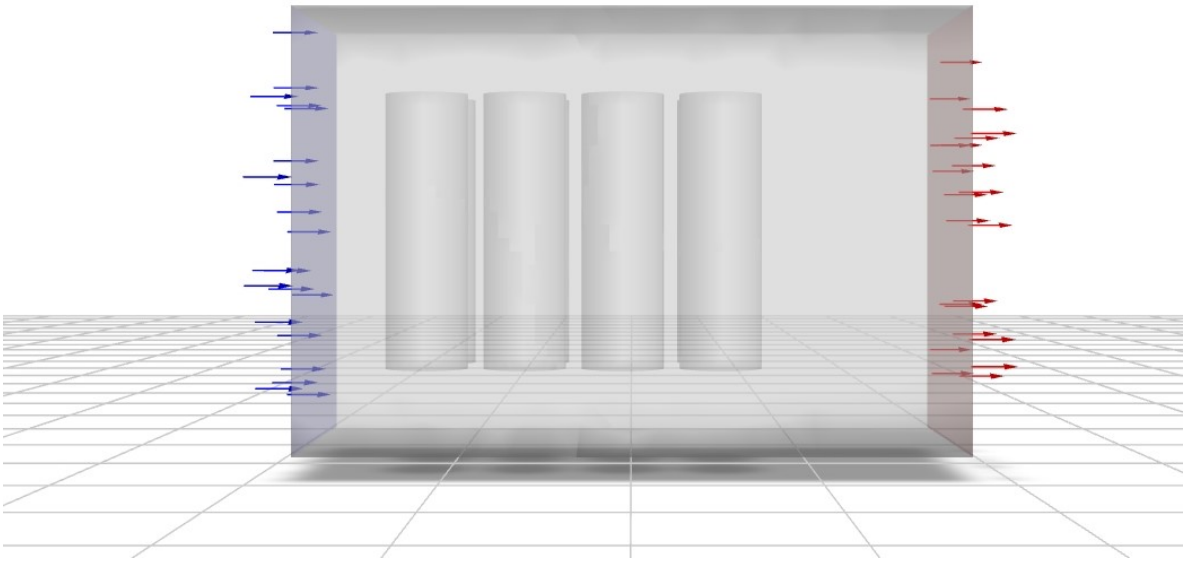

Figure 23: Schematic of forced convection

is added to the boundary conditions at the inlet. Moreover, to observe the outcome of heat dissipation in the fluid domain, the enclosure of the fluid domain in y-direction is kept bigger when compared to forced convection (refer to Figure 24). Ambient temperatures at different discharge rates are varied as boundary conditions. For the simulation of natural convection air is considered here as an incompressible fluid as the density varies with the temperature.

In the case of PCM cooling, Glycerol is used as the phase change material. From the literature review in section 2.9.3. It was drawn out that for the cooling of the Li-ion batteries, the preferred PCM should desirably have a melting point below 40^oC considering the operating temperature range. Supposing the example that the battery pack is to be used in the Netherlands, and the Netherlands has an annual average temperature of 12^oC - 13^oC the glycerol initially is going to stay in its solid state but as discharging of the batteries start and heat generation raises the system temperature glycerin will start to transition in liquid state.

3.7 Model Validation

The aim of the model validation is to demonstrate the precision of the numerical model that has been implemented. For the model validation average battery temperature for 1.5C discharge rate at 2 m/s inlet velocity and cell spacing of 2 mm at an ambient temperature of 24^oC for the validation of forced convection setup. The same

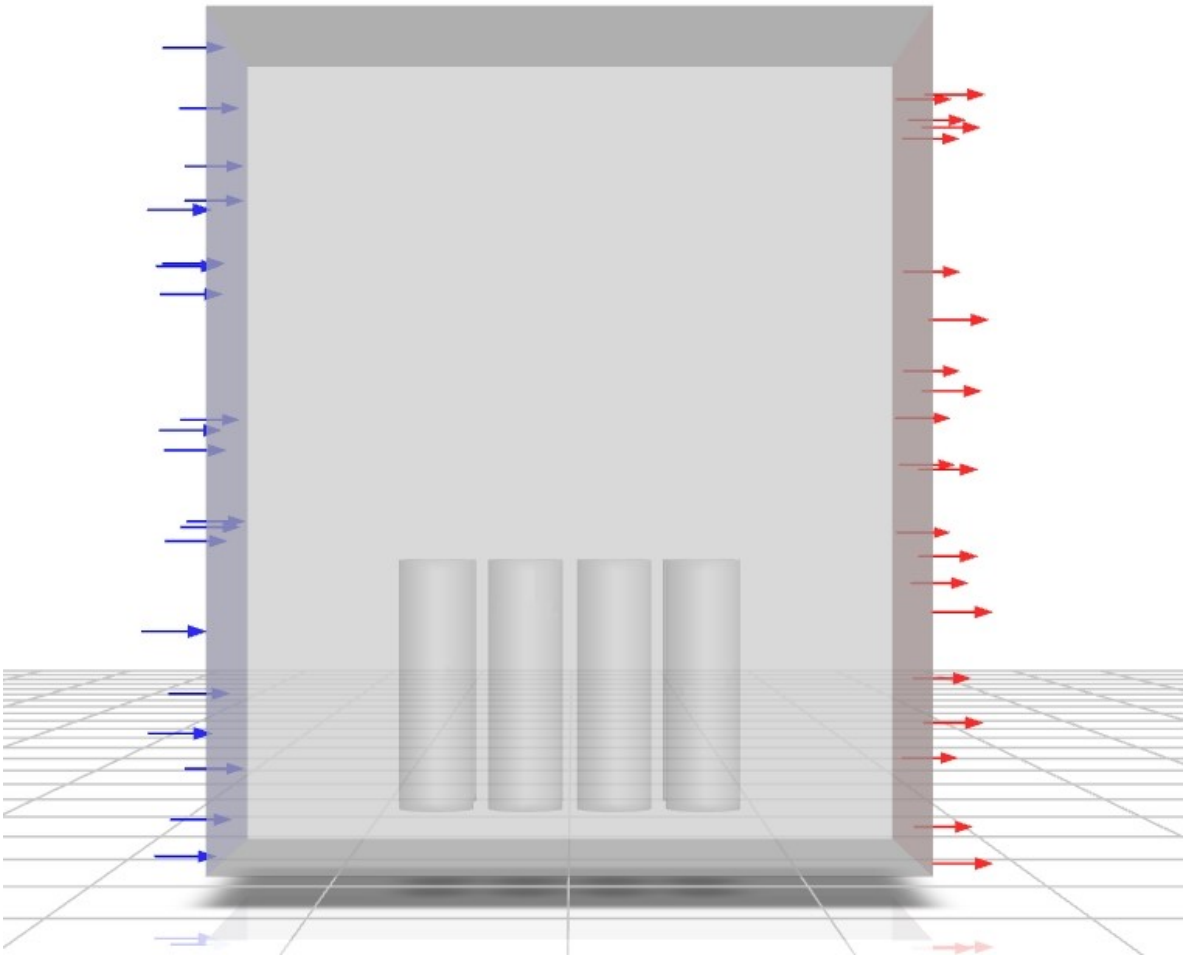

Figure 24: Schematic of natural convection

parameters have been considered to validate the model setup for natural convection. To validate the model used in this research the model used by Behi et al.[48] is used. The Li-ion battery used in their model is 18650 (3.6 V and 2.2 Ah) with the simulation performed at 26^oC at 1.5C discharge rate with an inlet velocity of 2 m/s and the spacing between the cells is 2 mm.

On comparison of the models, temperature follows the same trend as seen in Figure 25. and Figure 26. The average temperature is higher than the temperature measured by [48] as there is a difference between the cell geometry and capacity. The heat generation rate in the 21700 (3.7V and 4.5 Ah) is higher. So, the average temperature of the model is higher. More importantly, the model follows the trend line of the experimental data and simulation data of the compared model. So, it is safe to say that the results

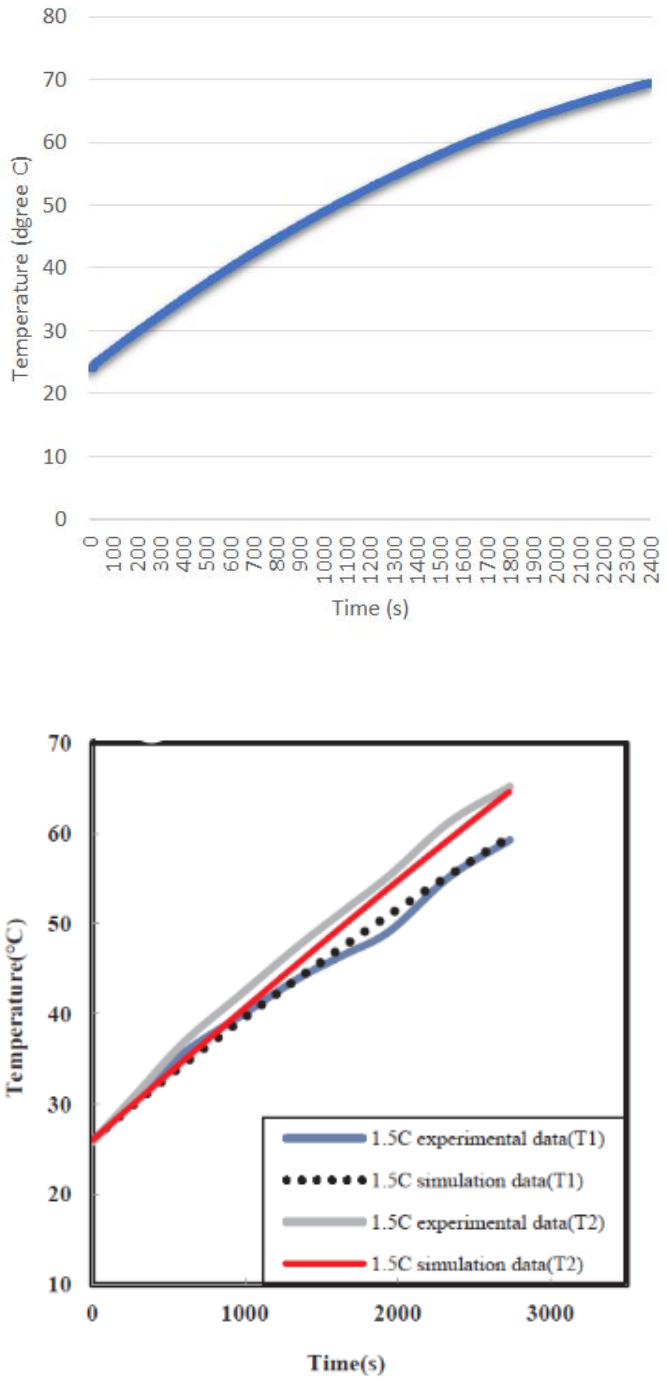

Figure 25: Thermal model validation for natural convection[48]

produced by the simulation models are quite accurate.

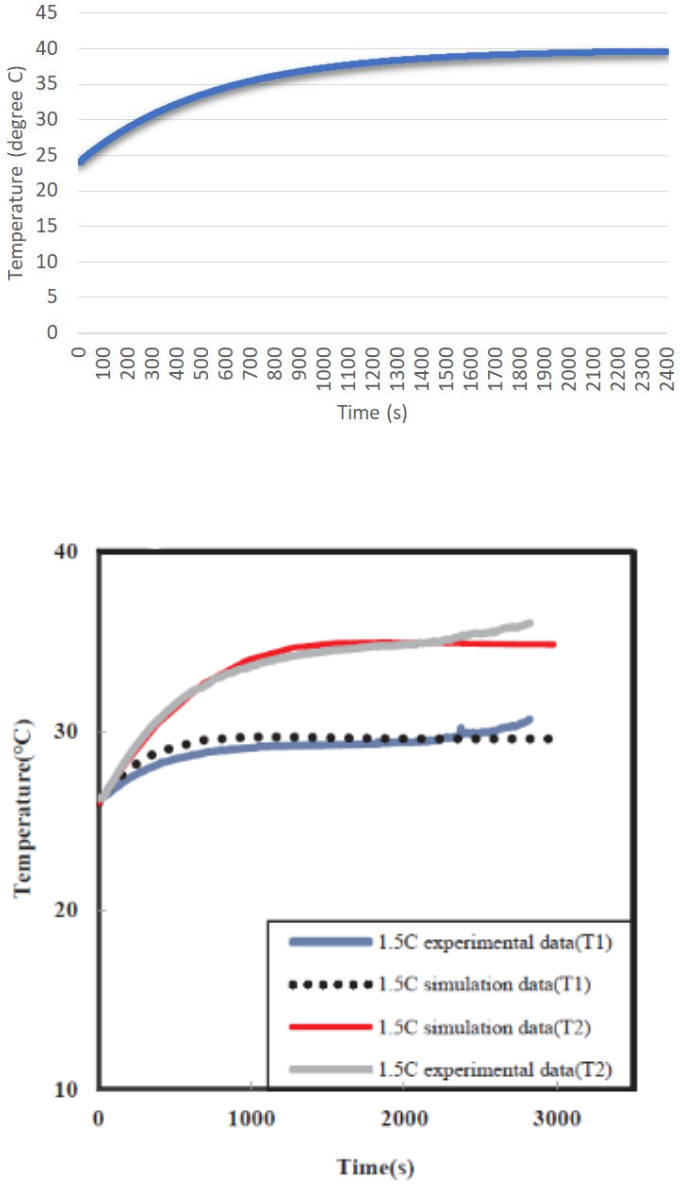

Figure 26: Thermal model validation for Forced convection[48]

4 Results

As discussed in the previous section, modules of 4S1P in parallel were studied. Apart from natural convection, forced convection cooling methods and cooling with the help of PCM were done in order to determine the thermal behaviour of Li-ion cells under various operating conditions with varied discharge rates. The findings about the variation in maximum, minimum, and temperature difference across the modules (ΔT) for different cooling methods are presented in Tables 12, 13, and 14.

Discharge Rate	Ambient Temperature	Max. Temperature	Min. Temperature	ΔT	
	0	46.81	35.864	10.946	
1.5C	24	72.296	61.574	10.722	
	35	83.966	73.329	10.637	
	0	31.587	25.114	6.473	
1C	24	53.504	46.74	6.764	2mm
	35	67.288	60.99	6.298	
	0	74.237	57.266	16.971	
2C	24	98.678	82.529	16.149	
	35	109.384	93.612	15.772	
	0	55.621	46.046	9.575	
1.5C	24	79.913	70.914	8.999	
	35	91.101	82.284	8.817	
	0	33.802	28.147	5.655	
1C	24	58.222	52.715	5.507	4mm
	35	69.425	63.995	5.43	
	0	78.296	64.448	13.848	
2C	24	102.588	89.501	13.087	
	35	113.676	100.889	12.787	
	0	55.385	42.932	12.453	
1.5C	24	79.057	66.634	12.423	
	35	90.207	78.116	12.091	
	0	32.753	26.585	6.168	
1C	24	56.868	50.889	5.979	6mm
	35	67.934	62.04	5.894	
	0	77.112	57.954	19.158	
2C	24	101.275	82.979	18.296	
	35	112.23	94.214	18.016	

Table 12: Effect of ambient temperature on battery modules during natural convection at different discharge rates

As is evident from Table 12. the values of the maximum temperature during different discharge rates go higher than the required safe operating temperature of the batter-

ies. The majority of the cases shown in the table are more likely to result in thermal runaway. This indicates that the cell modules in a 52V 18Ah battery pack under these operating conditions require an efficient battery thermal management system along with a cooling method that can be complied with easily. The visual representation of the temperature contours can be seen in Figures 27, 28, and 29. showing the temperature in the batteries when discharging at 2C during natural convection.

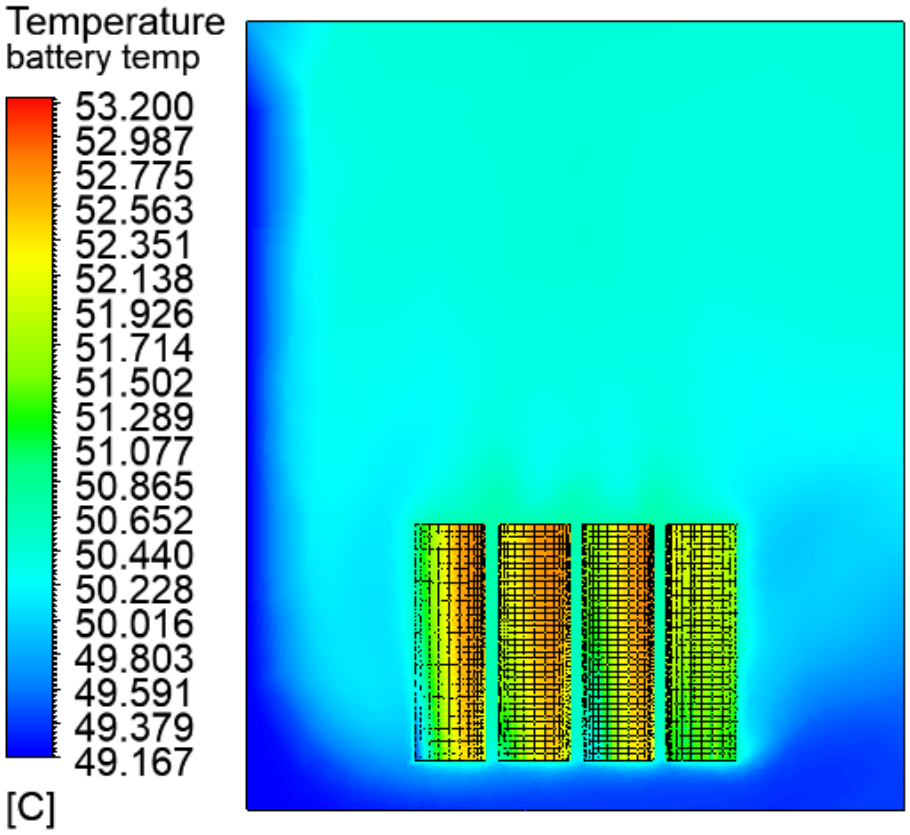

Figure 27: Natural Convection at 24^oC 2C discharge (T=10 minutes)

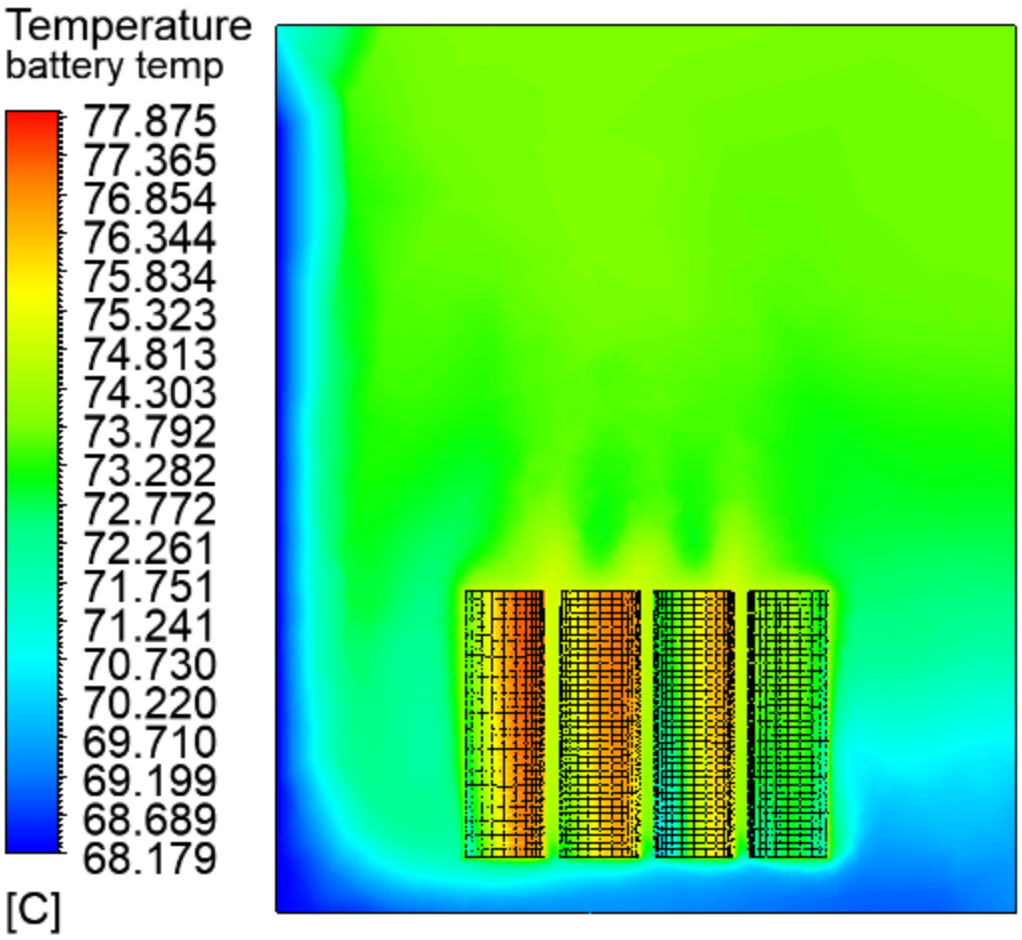

Figure 28: Natural Convection at 24^oC 2C discharge (T=20 minutes)

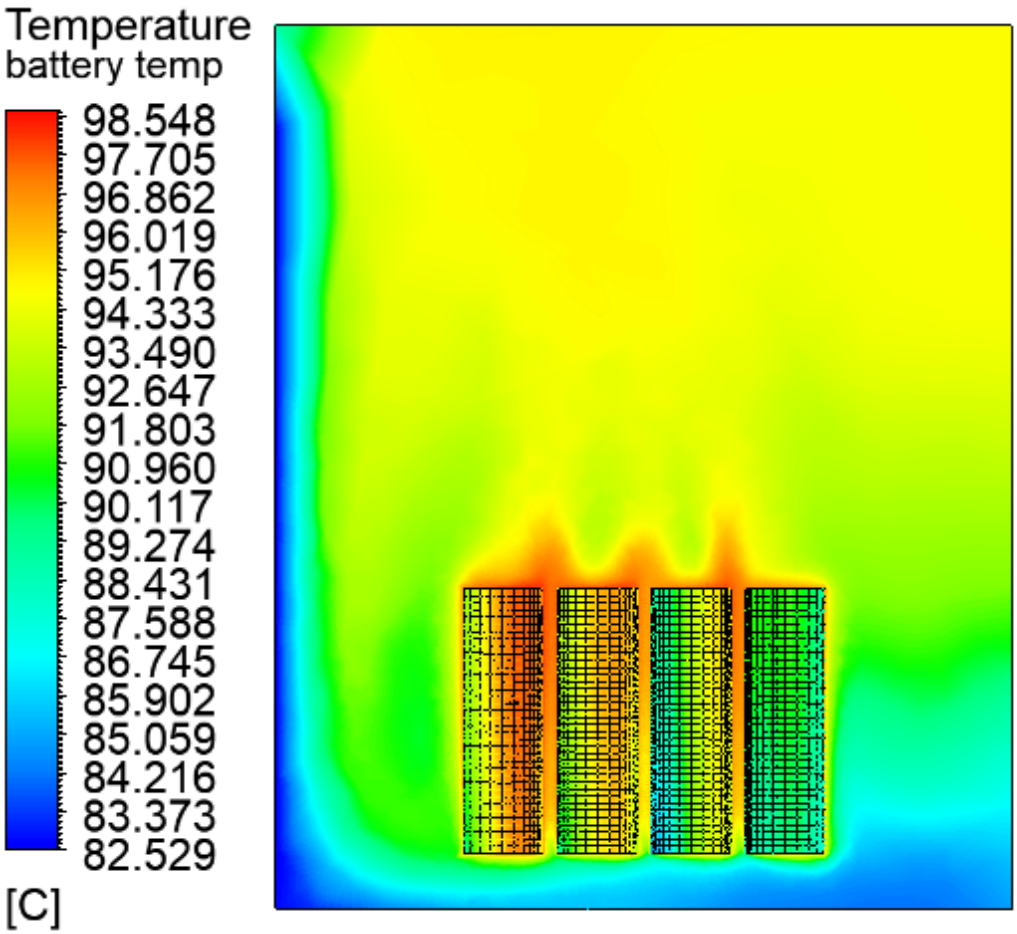

Figure 29: Natural Convection at 24^oC 2C discharge (T=30 minutes)

The pictures show the temperature contour of the batteries and surrounding air from the side view. The photos from different time steps show how the natural convection takes place over time at the ambient temperature of 24^oC. As depicted in the images the temperature of the air near the batteries starts to rise. Following that, the batteries are enveloped by a thin layer of elevated temperature and heat transfer initiates from this zone to other surrounding outer layers of the air. So, as the temperature of the air, adjacent to the batteries is higher the air density lowers. As the density of the heated air is lowered it tends to rise upwards which can be seen in the contours. The vector plot of the process shows how the air circulates during the process trying to cool the heated batteries. The vector plot for the natural convection at T=30 min is shown in Figure 30.

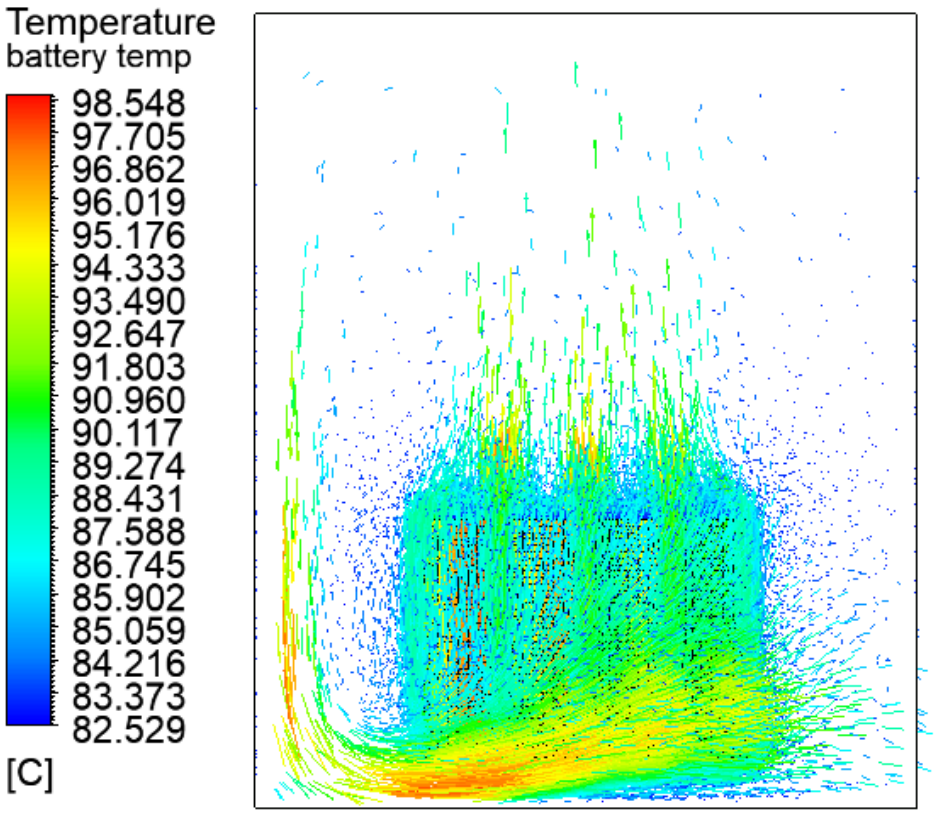

Figure 30: Vector Plot Natural Convection at 24^oC 2C discharge (T=30 minutes)

Discharge Rate	Inlet Velocities	Ambient Temperature	Max. Temperature	Min. Temperature	ΔT	
1C	1	24	34.728	28.683	6.045	2mm
	2	24	32.374	28.145	4.229	
	1	35	45.525	39.683	5.842	
	2	35	43.374	39.145	4.229	
1.5C	1	24	47.278	34.431	12.847	
	2	24	42.604	33.295	9.309	
	1	35	58.278	45.431	12.847	
	2	35	53.604	44.294	9.31	
2C	1	24	63.033	42.122	20.911	
	2	24	56.017	40.261	15.756	
	1	35	73.331	53.122	20.209	
	2	35	67.017	51.26	15.757	
1C	1	24	32.476	27.727	4.749	4mm
	2	24	30.341	27.171	3.17	
	1	35	43.078	38.656	4.422	
	2	35	41.341	38.171	3.17	
1.5C	1	24	42.783	32.343	10.44	
	2	24	38.25	31.084	7.166	
	1	35	53.783	43.343	10.44	
	2	35	49.264	42.134	7.13	
2C	1	24	56.313	38.625	17.688	
	2	24	48.982	36.448	12.534	
	1	35	67.313	49.625	17.688	
	2	35	59.982	47.448	12.534	
1C	1	24	32.326	27.914	4.412	6mm
	2	24	30.651	27.352	3.299	
	1	35	42.983	38.842	4.141	
	2	35	41.607	38.314	3.293	
1.5C	1	24	41.972	32.646	9.326	
	2	24	38.795	31.453	7.342	
	1	35	52.955	43.645	9.31	
	2	35	49.846	42.46	7.386	
2C	1	24	55.956	39.373	16.583	
	2	24	50.306	37.252	13.054	
	1	35	66.956	50.373	16.583	
	2	35	61.396	48.266	13.13	

Table 13: Effect of inlet velocities and ambient temperature on battery modules during forced convection at different discharge rates

From the results of the forced convection obtained in Table 13. it is observed that

for given discharge rates at any ambient temperature when the velocity is increased the temperature difference (ΔT) in the modules is decreased. The schematics of the airflow showing the streamlines at 1C discharge rate and 35^oC with varying cell spacing are shown in Figure 31, 32, and 33.

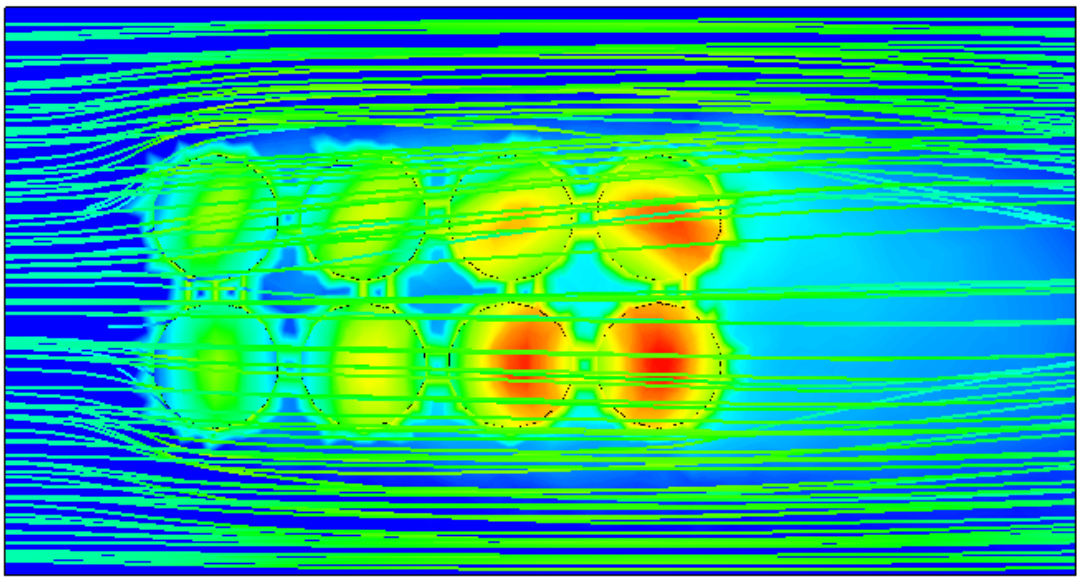

Figure 31: Flow lines at 1C discharge and 35^oC with 2mm cell spacing

As observed in the streamline schematics at different cell spacing the heating due to the heat of adjacent cells decreases as the cell spacing increases. As the cell spacing increases the amount of air flowing through the spaces or gaps between the batteries also increases which leads to better cooling of the cells. Comparing the temperature plot of the batteries, in the 2mm cell spacing the last three batteries heat up displaying non-uniformity of the temperature. While temperature plots for 4mm and 6mm cell spacing show better uniformity of the temperature across the modules.

Another observation that is made from the table is that with the rise in the inlet velocity at the constant ambient temperature and discharge rate, the maximum temperature of the modules decreases by $2-3^oC$ for 1C and 1.5C discharge with 2mm spacing. For the same cell spacing at the higher discharge rate of 2C, the maximum temperature drops by almost 7^oC. When the cell spacing is increased to 4mm, the maximum temperature of the modules is decreased by 2^oC, 4.5^oC, and 7^oC for 1C, 1.5C, and 2C discharge rates respectively. Much better cooling is observed with the increase in cell spacing to 6mm.

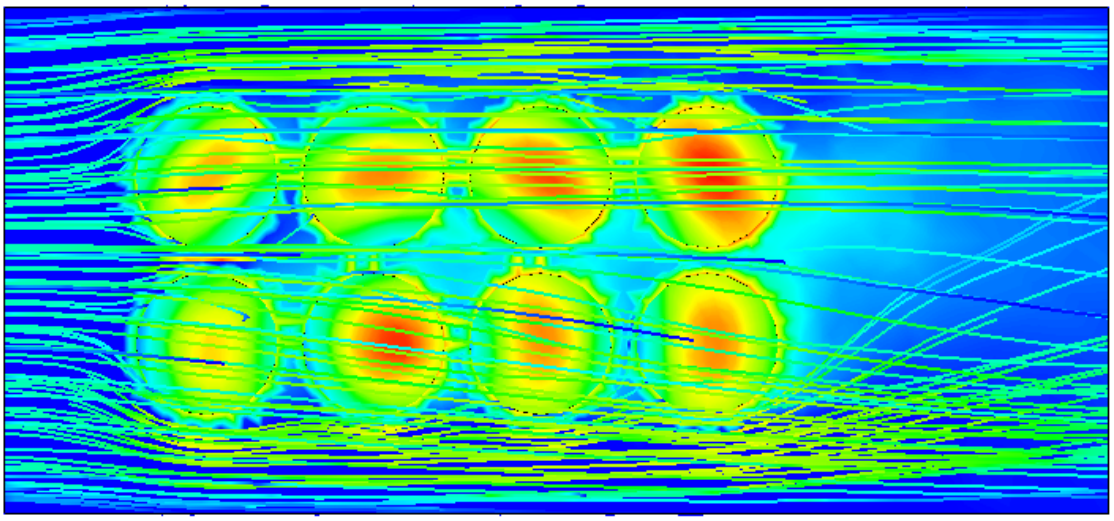

Figure 32: Flow lines at 1C discharge and 35^oC with 4mm cell spacing

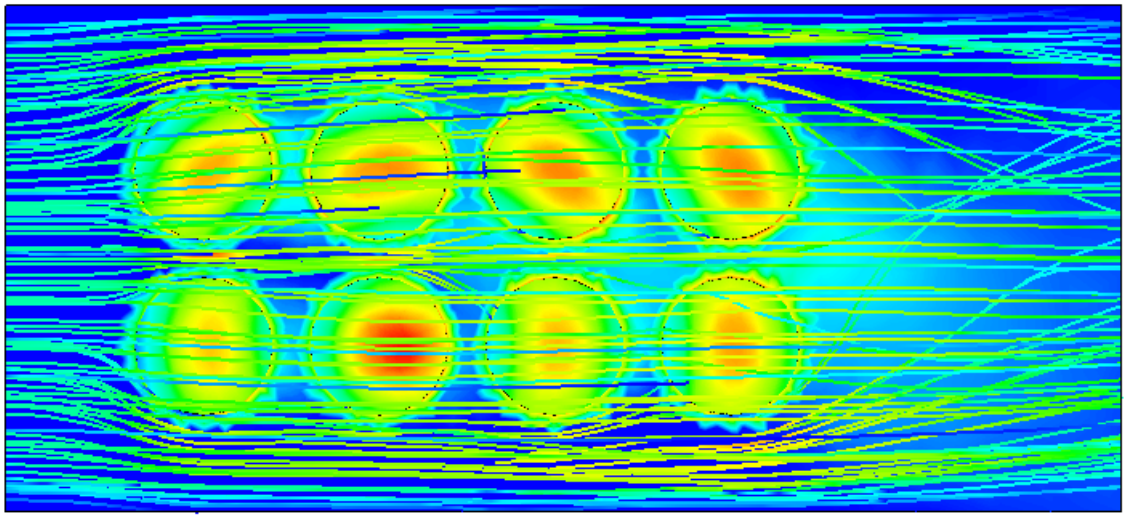

Figure 33: Flow lines at 1C discharge and 35^oC with 6mm cell spacing

In the simulation setup for the forced convection an assumption was made, as the velocities used are very low the flow was assumed to be laminar despite Re=54,501. To compare and see the deviation in results a simulation model with a turbulent setup was investigated. The boundary conditions for both laminar and turbulent models were taken as; 2C discharge with an inlet velocity of 2 m/s at 24^oC with cell spacing of 4mm was considered. Figures 34. and 35. visually show the behaviour of air to cool the modules. The temperature difference of 1.587^oC was observed between both flows. Considering the simulation just for the modules, the difference is not significant. How-

ever, if the simulation is to be performed on the entire battery pack turbulent model is to be used for accurate results.

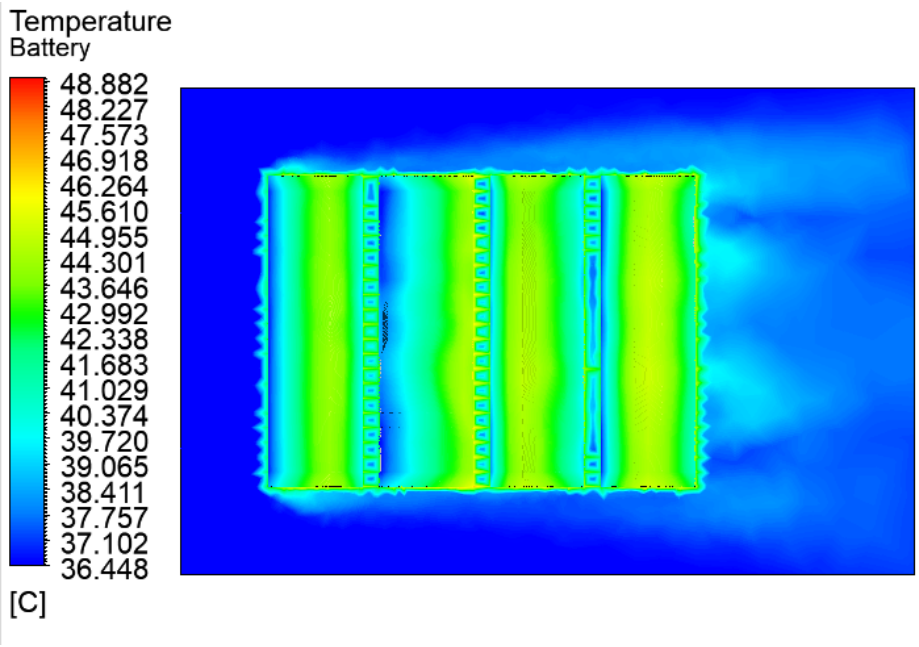

Figure 34: Laminar airflow

The forced convection cooling at low discharge rates and low inlet velocities of 1 and 2 m/s offer adequate cooling of batteries and a good temperature distribution along the modules. For higher discharge rates higher inlet velocities ranging from the 8-12 m/s can provide efficient cooling. Out of all cell spacing, the best cooling performance in all scenarios is seen in 6mm cell spacing. On comparing the results of ΔT for 4mm and 6mm spacing, no significant difference is observed. Hence while designing the battery pack, according to its application optimum cell spacing can be chosen for efficient cooling. As better cooling performance comes at the expense of an increase in the space of the battery pack.

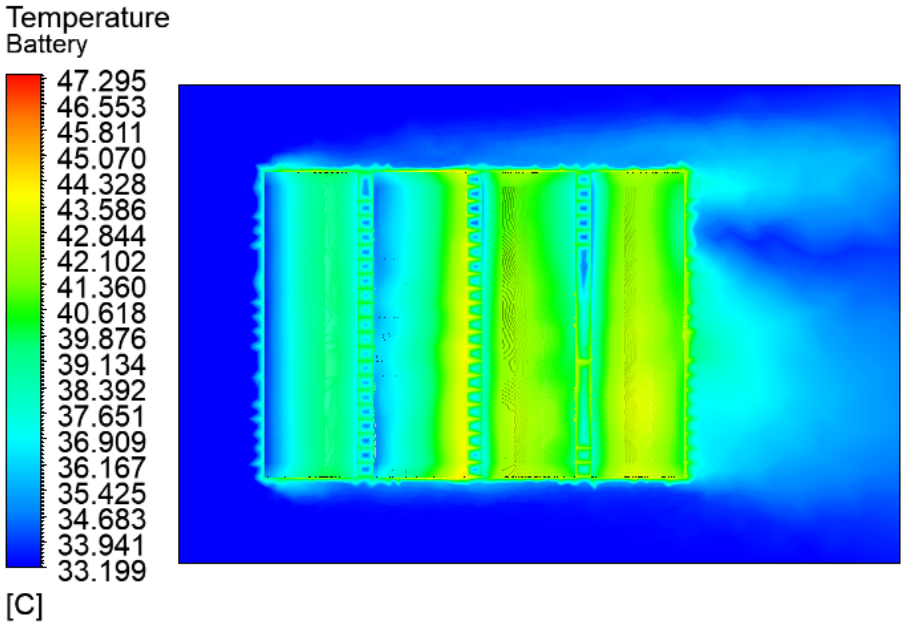

Figure 35: Turbulent airflow

Discharge Rate	Ambient Temperature	Max. Temperature	Min. Temperature	ΔT	
	0	19.822	8.7369	11.0851	
1.5C	24	39.894	30.164	9.73	
	35	50.772	41.145	9.627	
	0	11.998	4.772	7.226	
1C	24	32.931	24	8.931	2mm
	35	43.895	38.621	5.274	
	0	24.07	12.255	11.815	
2C	24	49.163	33.539	15.624	
	35	58.724	43.777	14.947	
	0	19.907	8.651	11.256	
1.5C	24	38.932	28.536	10.396	
	35	49.826	39.522	10.304	
	0	12.097	4.6159	7.4811	
1C	24	32.404	26.65	5.754	4mm
	35	43.345	37.646	5.699	
	0	24.731	12.066	12.665	
2C	24	46.431	30.536	15.895	
	35	57.38	41.512	15.868	

	0	19.093	8.334	10.759	
1.5C	24	38.172	30.077	8.095	
	35	49.025	41.061	7.964	
	0	10.935	4.5209	6.4141	
1C	24	31.771	27.505	4.266	6mm
	35	42.766	38.501	4.265	
	0	24.186	12.208	11.978	
2C	24	45.548	32.804	12.744	
	35	56.122	43.764	12.358	

Table 14: Effect of ambient temperature on battery modules cooling by PCM (Glycerol) at different discharge rates

From Table 14. it can be drawn out that Glycerol as a PCM gives the best cooling performance at 24^oC and 35^oC at 6mm cell spacing at 1C discharge. The results show that the used PCM keeps the maximum temperature of the battery modules below 60^oC (recommended battery temperature range by the manufacturer during discharge -40^oC - 60^oC) even at high discharge rates and ambient temperature. As observed from the results when compared to forced convection cooling, PCM seems to have better performance in reducing the maximum temperature of the modules at higher C-rates, and ambient temperature. The comparison of maximum temperatures can be seen in Figures 36 and 37.

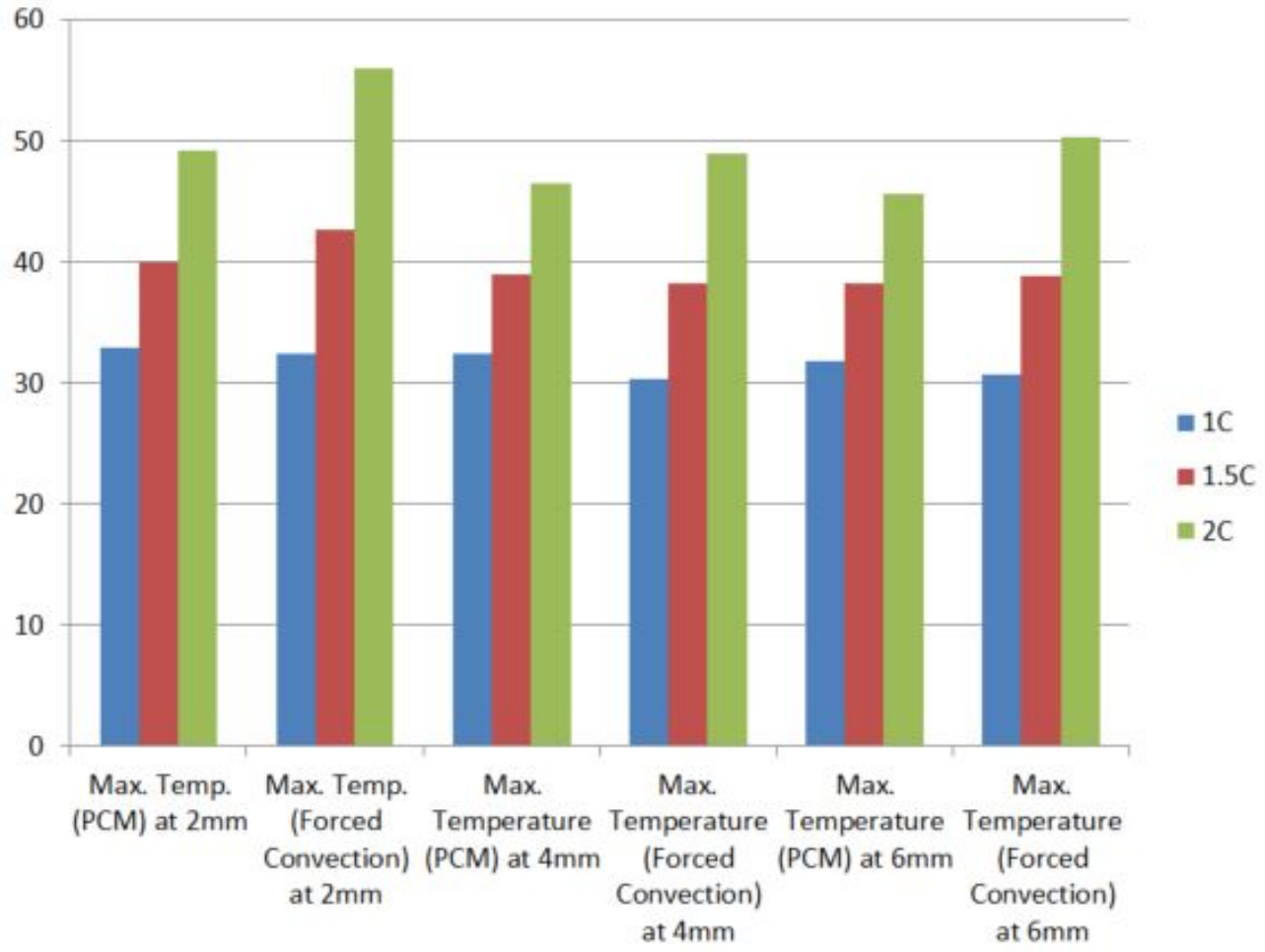

Figure 36: Comparison of maximum temperature at 24^oC between PCM and Forced convection

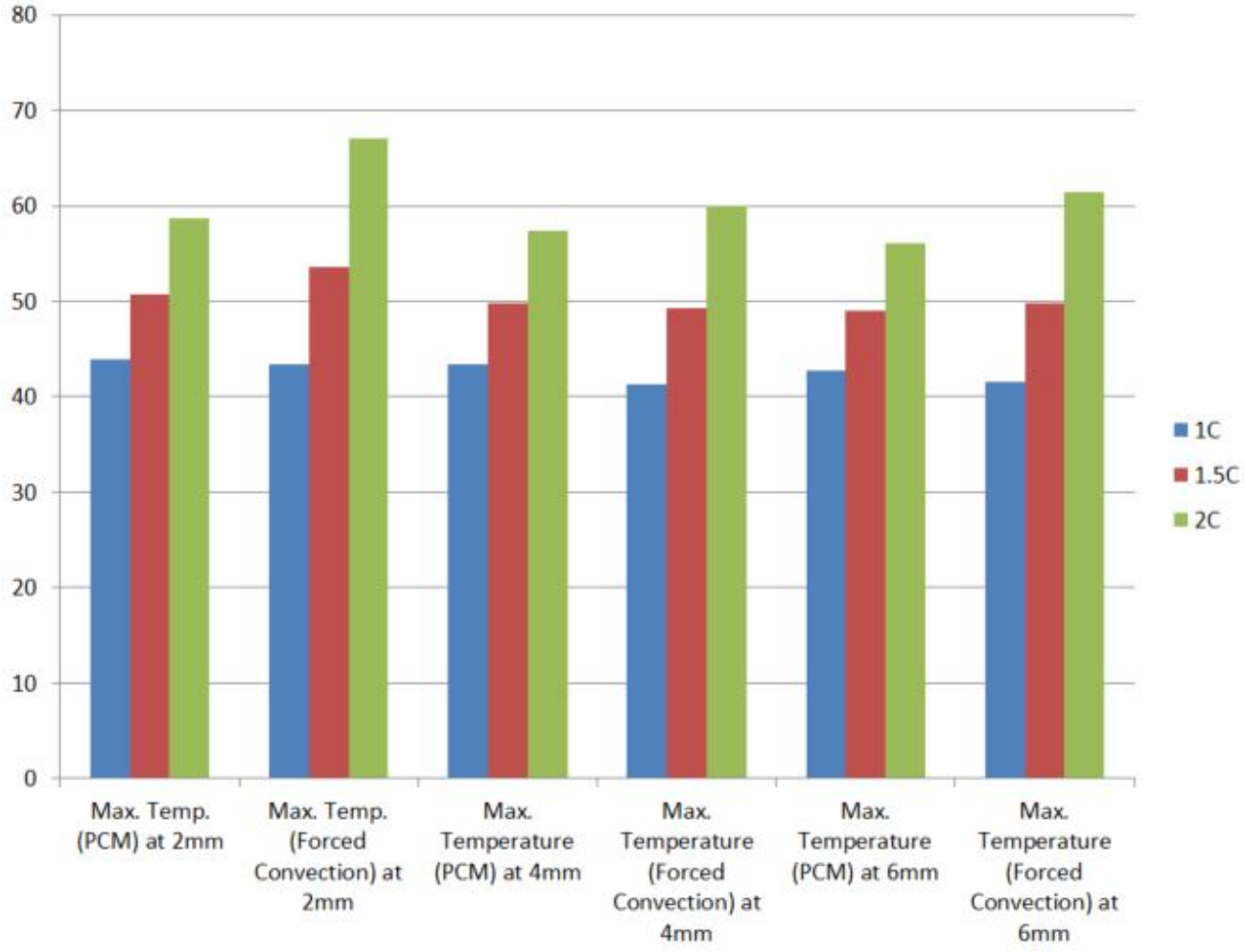

Figure 37: Comparison of maximum temperature at 35^oC between PCM and Forced convection

Glycerol as a PCM can be useful in the application of cooling batteries with relatively low heat generation rates. At 0^oC and 1C discharge rate the temperature of the batteries lies in the range of 4^oC to 12^oC, which is out of the optimal operating temperature range and can lead to reduced battery performance. This is due to glycerol staying in its solid state. Also, glycerol has the characteristics of supercooling (when a PCM fails to undergo phase change at the specified melting point). This affects the dissipation of heat from the battery modules. To understand the behavior of the PCM and how it affects the cooling of the batteries in their solid state and in, their liquid state. The data for the comparison is taken for the batteries at 1C discharge rate at 0^oC and 24^oC with cell spacing of 2mm. As can be seen in the figures below over time when glycerol is in its liquid state, the fluid surrounding the battery conducts the heat, and the heat is then conducted by other cold layers in it. While at 0^oC glycerin is in its solid state, it absorbs the heat uniformly as seen in the Figure 43.

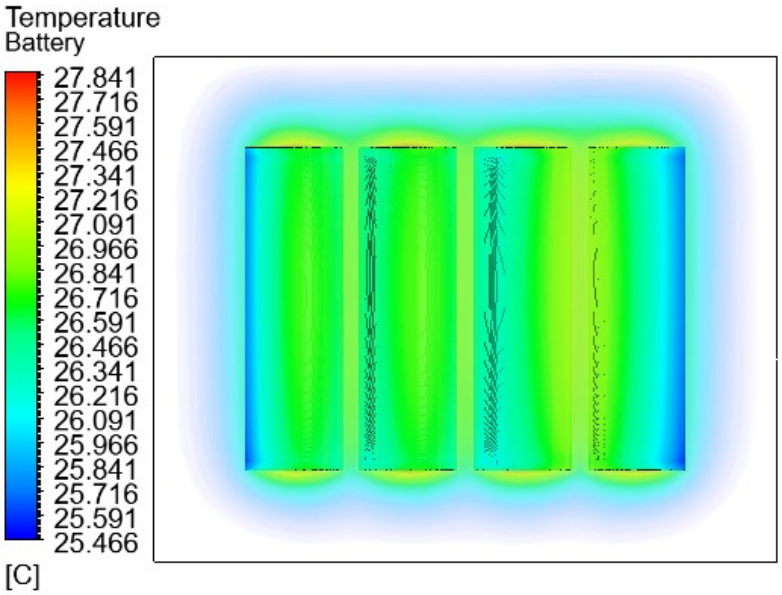

Figure 38: PCM at 24^oC 1C discharge (T=10 minutes)

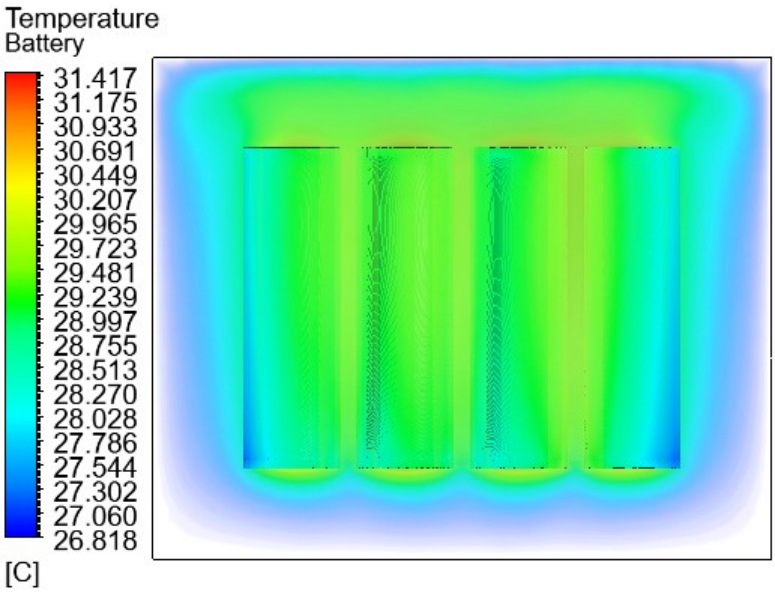

Figure 39: PCM at 24^oC 1C discharge (T=30 minutes)

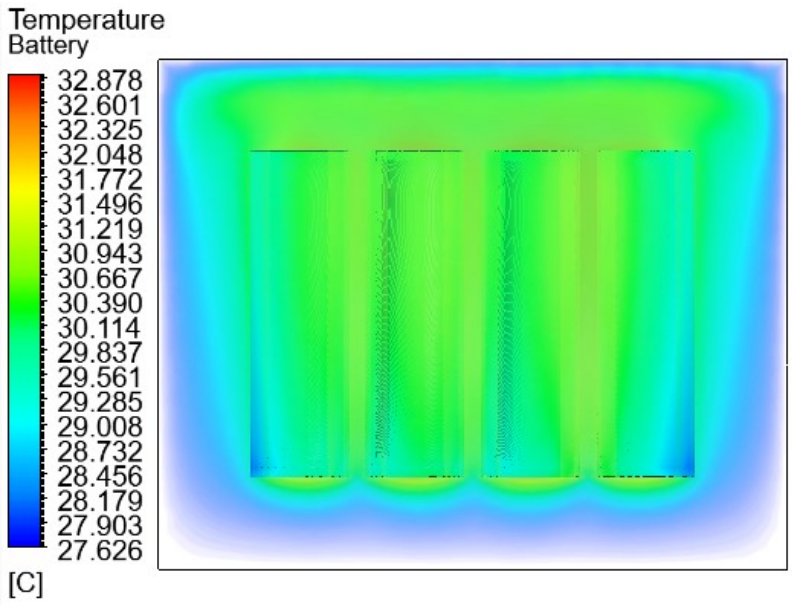

Figure 40: PCM at 24^oC 1C discharge (T=60 minutes)

Figure 38, 39, and 40 show the influence of PCM while the battery is discharging at 1C rate over time. These pictures show the behaviour of the PCM when it is in a liquid state.

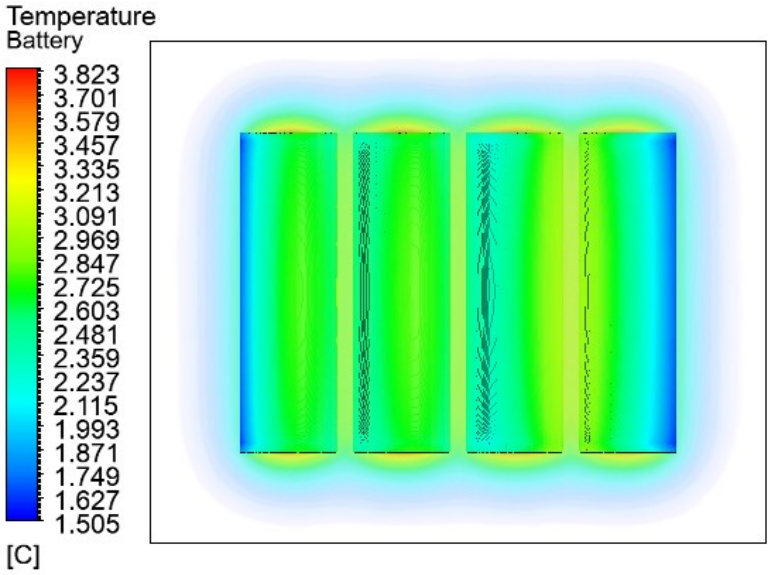

Figure 41: PCM at 0^oC 1C discharge (T=10 minutes)

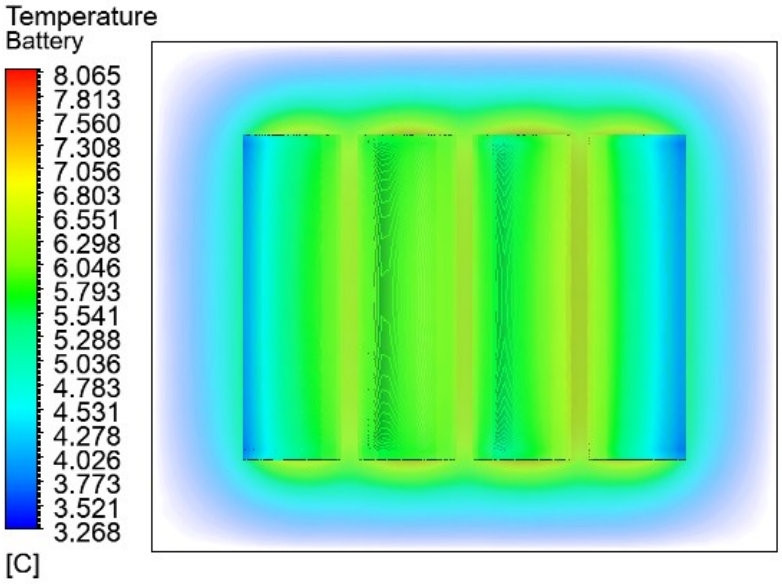

Figure 42: PCM at 0^oC 1C discharge (T=30 minutes)

Figure 41, 42, and 43 show the influence of PCM while the battery is discharging at 1C rate over time. These pictures show the behaviour of the PCM when it is in its solid state.

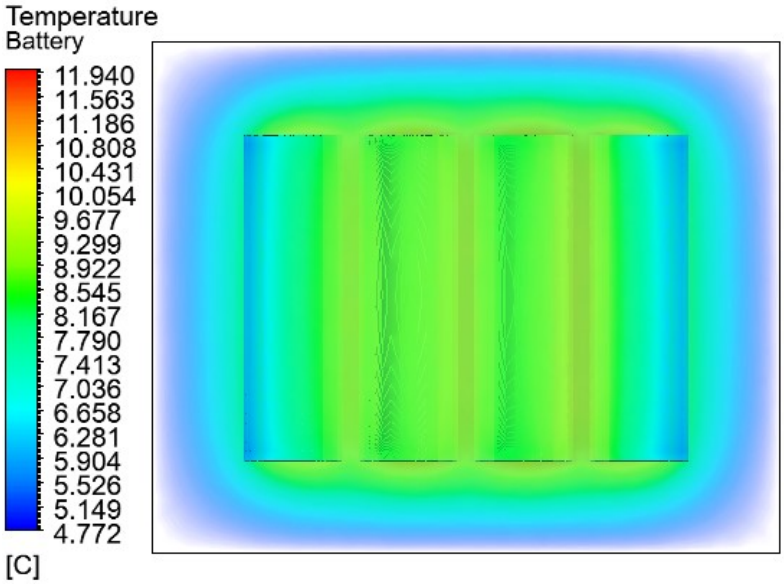

Figure 43: PCM at 0^oC 1C discharge (T=60 minutes)

Figures 44 and 45. shows the comparison of ΔT in cooling methods at 24^oC and 35^oC. On seeing both the graphs it is visible that forced air cooling provides the best uniformity of temperature across the modules followed by PCM (Glycerin) and then by natural convection.

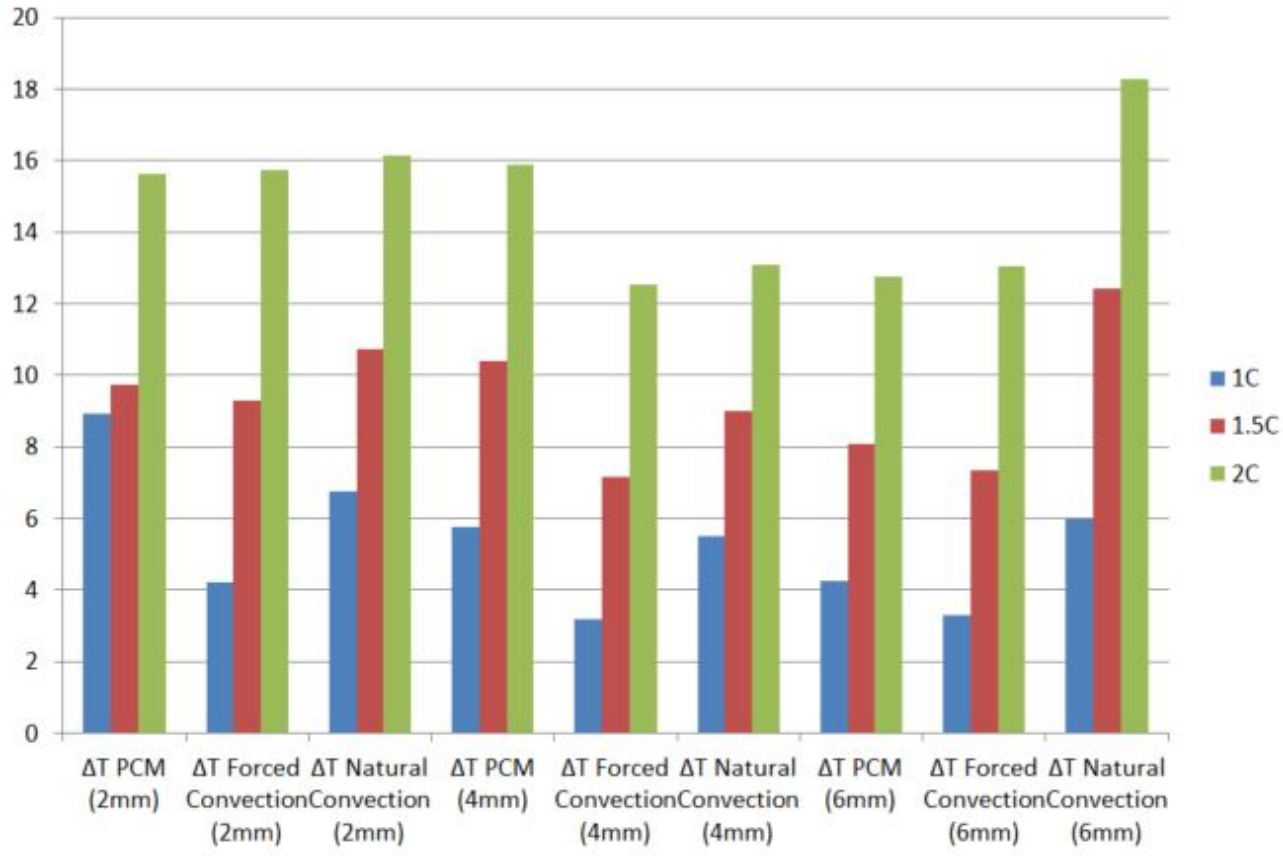

Figure 44: Comparison of ΔT at 24^oC in all cooling methods

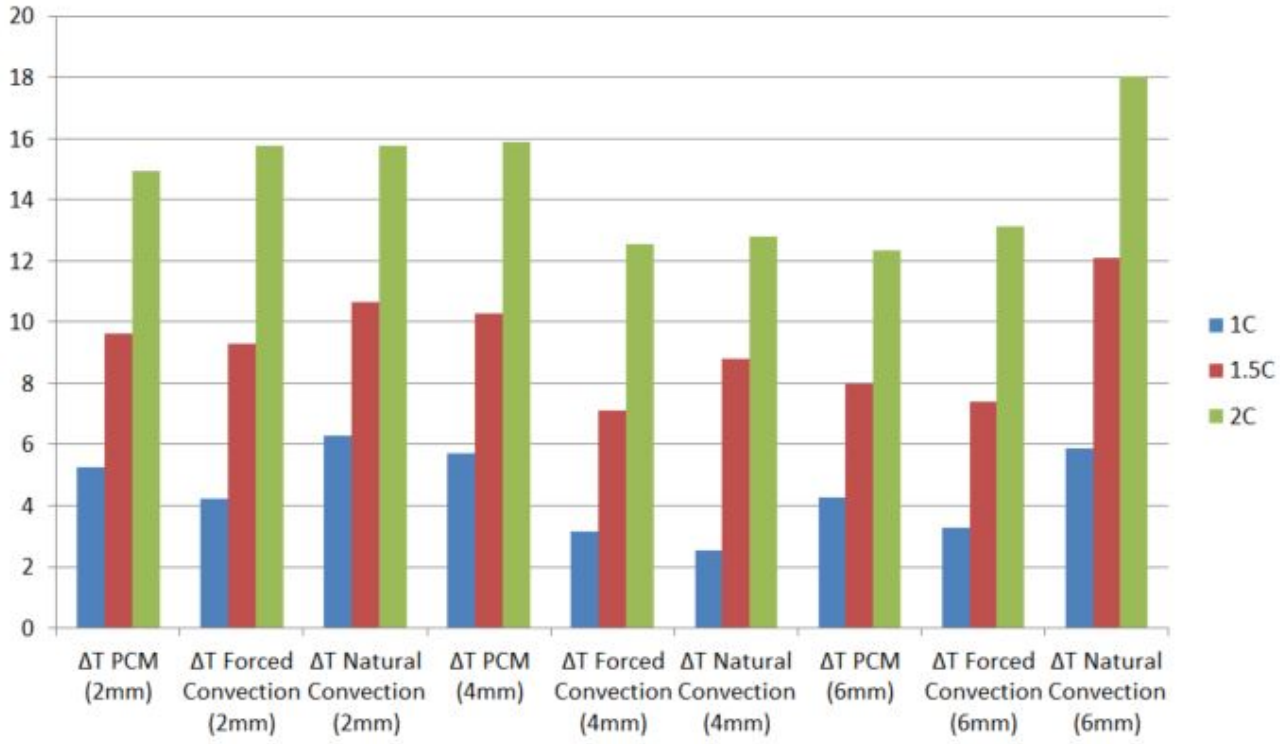

Figure 45: Comparison of ΔT at 35^oC in all cooling methods

5 Conclusion

The CFD thermal simulation of the 4S1P modules of 21700 lithium-ion batteries provided some critical insights regarding the cooling methods investigated. The investigation scenarios include the cooling of the modules by natural convection, forced convection, and cooling by PCM. All the research objectives set were fulfilled by the study. The results from the simulations are found to be in complete agreement with the literature review and match the results.

The simulation of the natural convection was to understand and observe the thermal behavior of the battery module if no cooling was applied to the battery. The results showed that without an optimal battery thermal management system it is very difficult to use batteries with such a capacity for desired applications. The simulation results show that the forced air cooling performs the best under a low discharge rate at low inlet velocity. verifying the information from the literature review for higher discharge rates or (C-rates), the air cooling can still perform with similar efficiency by providing higher inlet velocities. studying the results of the forced convection, to increase the uniformity throughout the battery pack, the position of the inlet can be changed to the top of the batteries. The air flowing from the top and venting out from the horizontal direction can lead to the recirculation of air inside the pack and can be helpful in the removal of the heat.

The turbulent system model was compared with the assumed laminar flow model to check the deviations. Seeing the results of both simulations on a modular level it is okay to assume the laminar flow to reduce the computation time. However, in a pack-level simulation, it is highly recommended to use the turbulent model if Reynold's number lies in the turbulent range. Studying the results of the cooling via PCM, it can be said that glycerin is definitely not the right material for the cooling of the battery packs based on the desired application. Although it had positive signs showing better performance in lowering the maximum temperature in comparison to air cooling. Also, it can be concluded that PCM with less difference in their phase change temperature does not particularly perform better in storing or releasing the heat. But with new materials engineered, nanoparticles or graphite mixed with the paraffin to alter the heat-carrying capacity of the material can be used to investigate the thermal behaviour of PCMs more.

Lastly, there's no effective BTMS solution that can fit into all the ranges of applications. So, it is better to focus on developing efficient BTMS focusing on a specific range of applications and requirements. Factors like cost, life cycle, manufacturability, safety, impact on the environment, etc. are to be considered before choosing the cooling methods for designing a thermal management system.

6 Future Recommendations

Based on the important observations from the results of forced convection and cooling by PCM, a hybrid cooling mechanism involving the use of forced convection and PCM can be investigated based on the application of the battery pack. As glycerin showed the potential to lower the maximum temperature of the modules, forced convection has shown better results with better temperature uniformity in comparison to other cooling methods. This thermal simulation provides good insights to a designer who is designing BTMS. But for future work, equivalent circuit models or other coupled models can be simulated to study the parameters such as SOC, variable resistances, dynamic loading conditions, etc. If designing a thermal management system for a higher range of battery pack applications liquid cooling with a bottom plate or heat blocks containing mini channels can be investigated.

Bibliography

[1] Chai Siang Cheng. *Design, development and analysis of a battery electric vehicle energy storage system*. PhD thesis, 2017.

[2] VĂSCAN Iulia and SZABÓ Loránd. A brief history of electric vehicles. *Journal of Computer Science & Control Systems*, 15(1), 2022.

[3] Trend Investing. A look at the top 5 lithium-ion battery manufacturers in 2019 — seeking alpha. https://seekingalpha.com/article/4289626-look-top-5-lithium-ion-battery-manufacturers-in-2019, 2023. Accessed: 2023-09-11.

[4] Christopher Hendricks, Nick Williard, Sony Mathew, and Michael Pecht. A failure modes, mechanisms, and effects analysis (fmmea) of lithium-ion batteries. *Journal of Power Sources*, 297:113–120, 2015.

[5] Qingsong Wang, Ping Ping, Xuejuan Zhao, Guanquan Chu, Jinhua Sun, and Chunhua Chen. Thermal runaway caused fire and explosion of lithium ion battery. *Journal of power sources*, 208:210–224, 2012.

[6] Sharon S Chadwick. Ullmann's encyclopedia of industrial chemistry. *Reference Services Review*, 16(4):31–34, 1988.

[7] PortaSpecs. Power of the future: Uncovering the secrets of the nca battery. https://www.portaspecs.com/power-of-the-future-uncovering-the-secrets-of-the-nca-battery/, 2023. Accessed: 2023-09-11.

[8] Henrik Lundgren, Pontus Svens, Henrik Ekström, Carl Tengstedt, Johan Lindström, Mårten Behm, and Göran Lindbergh. Thermal management of large-format prismatic lithium-ion battery in phev application. *Journal of The Electrochemical Society*, 163(2):A309, 2015.

[9] Designed and www.maharashtradirectory.com Promoted by Maharashtra Industries Directory. Electro oxidation from pune, maharashtra, india. https://www.aquacaresee.co.in/electro-oxidation.html, 2023. Accessed: 2023-09-11.

[10] Walter Van Schalkwijk and Bruno Scrosati. Advances in lithium ion batteries introduction. In *Advances in lithium-ion batteries*, pages 1–5. Springer, 2002.

[11] Anne De Guibert. Batteries and supercapacitor cells for the fully electric vehicle. In *Proc. Smart Syst. Integr. Conf*, 2009.

[12] K Brandt. Historical development of secondary lithium batteries. *Solid State Ionics*, 69(3-4):173–183, 1994.

[13] Xuning Feng, Minggao Ouyang, Xiang Liu, Languang Lu, Yong Xia, and Xiangming He. Thermal runaway mechanism of lithium ion battery for electric vehicles: A review. *Energy storage materials*, 10:246–267, 2018.

[14] Xuning Feng, Siqi Zheng, Dongsheng Ren, Xiangming He, Li Wang, Hao Cui, Xiang Liu, Changyong Jin, Fangshu Zhang, Chengshan Xu, et al. Investigating the thermal runaway mechanisms of lithium-ion batteries based on thermal analysis database. *Applied Energy*, 246:53–64, 2019.

[15] Niels Gartner. Thermal behaviour of lithium-ion batteries and the implications on submarine system design. 2021.

[16] Bruce Dunn, Haresh Kamath, and Jean-Marie Tarascon. Electrical energy storage for the grid: a battery of choices. *Science*, 334(6058):928–935, 2011.

[17] Christian Julien, Alain Mauger, Ashok Vijh, Karim Zaghib, Christian Julien, Alain Mauger, Ashok Vijh, and Karim Zaghib. *Lithium batteries*. Springer, 2016.

[18] Yuqiong Kang, Zheng Liang, Yun Zhao, Haiping Xu, Kun Qian, Xiangming He, Tao Li, and Jiangang Li. . *Science China Materials*, 63:1683–1692, 2020.

[19] Christian Julien, Alain Mauger, Ashok Vijh, Karim Zaghib, Christian Julien, Alain Mauger, Ashok Vijh, and Karim Zaghib. Principles of intercalation. *Lithium Batteries: Science and Technology*, pages 69–91, 2016.

[20] LHJ Raijmakers, DL Danilov, R-A Eichel, and PHL Notten. A review on various temperature-indication methods for li-ion batteries. *Applied energy*, 240:918–945, 2019.

[21] Qian Wang, Bin Jiang, Bo Li, and Yuying Yan. A critical review of thermal management models and solutions of lithium-ion batteries for the development of pure electric vehicles. *Renewable and Sustainable Energy Reviews*, 64:106–128, 2016.

[22] Thomas B Reddy. *Linden's handbook of batteries*. McGraw-Hill Education, 2011.

[23] Qingsong Wang, Binbin Mao, Stanislav I Stoliarov, and Jinhua Sun. A review of lithium ion battery failure mechanisms and fire prevention strategies. *Progress in Energy and Combustion Science*, 73:95–131, 2019.

[24] Bin Xu, Jinwoo Lee, Daeil Kwon, Lingxi Kong, and Michael Pecht. Mitigation strategies for li-ion battery thermal runaway: A review. *Renewable and Sustainable Energy Reviews*, 150:111437, 2021.

[25] Yuqing Chen, Yuqiong Kang, Yun Zhao, Li Wang, Jilei Liu, Yanxi Li, Zheng Liang, Xiangming He, Xing Li, Naser Tavajohi, et al. A review of lithium-ion battery safety concerns: The issues, strategies, and testing standards. *Journal of Energy Chemistry*, 59:83–99, 2021.

[26] Manh-Kien Tran, Anosh Mevawalla, Attar Aziz, Satyam Panchal, Yi Xie, and Michael Fowler. A review of lithium-ion battery thermal runaway modeling and diagnosis approaches. *Processes*, 10(6):1192, 2022.

[27] Donal P Finegan, Eric Darcy, Matthew Keyser, Bernhard Tjaden, Thomas MM Heenan, Rhodri Jervis, Josh J Bailey, Nghia T Vo, Oxana V Magdysyuk, Michael Drakopoulos, et al. Identifying the cause of rupture of li-ion batteries during thermal runaway. *Advanced Science*, 5(1):1700369, 2018.

[28] Kai Liu, Yayuan Liu, Dingchang Lin, Allen Pei, and Yi Cui. Materials for lithium-ion battery safety. *Science advances*, 4(6):eaas9820, 2018.

[29] John T Warner. *Lithium-ion battery chemistries: a primer*. Elsevier, 2019.

[30] Andrey W Golubkov, René Planteu, Philipp Krohn, Bernhard Rasch, Bernhard Brunnsteiner, Alexander Thaler, and Viktor Hacker. Thermal runaway of large automotive li-ion batteries. *RSC advances*, 8(70):40172–40186, 2018.

[31] Andrey W Golubkov, David Fuchs, Julian Wagner, Helmar Wiltsche, Christoph Stangl, Gisela Fauler, Gernot Voitic, Alexander Thaler, and Viktor Hacker. Thermal-runaway experiments on consumer li-ion batteries with metal-oxide and olivin-type cathodes. *Rsc Advances*, 4(7):3633–3642, 2014.

[32] Aron Saxon, Mitchell Powell, and Ying Shi. Battery thermal characterization. Technical report, National Renewable Energy Lab.(NREL), Golden, CO (United States), 2015.

[33] Yan Ji and Chao Yang Wang. Heating strategies for li-ion batteries operated from subzero temperatures. *Electrochimica Acta*, 107:664–674, 2013.

[34] Ian Hunt. Thermal effects and management of lithium ion batteries for automotive applications. 2017.

[35] Jean Baptiste Joseph Fourier. *Théorie analytique de la chaleur*. Gauthier-Villars et fils, 1888.

[36] Venkat Srinivasan and Chao-Yang Wang. Analysis of electrochemical and thermal behavior of li-ion cells. *Journal of The Electrochemical Society*, 150(1):A98, 2002.

[37] The application of numerical methods in heat transfer problems — system analysis blog — cadence. https://resources.system-analysis.cadence.com/blog/msa2022-the-application-of-numerical-methods-in-heat-transfer-problems, 2023. Accessed: 2023-09-12.

[38] Kai Chen, Yiming Chen, Zeyu Li, Fang Yuan, and Shuangfeng Wang. Design of the cell spacings of battery pack in parallel air-cooled battery thermal management system. *International Journal of Heat and Mass Transfer*, 127:393–401, 2018.

[39] Chunrong Zhao, Wenjiong Cao, Ti Dong, and Fangming Jiang. Thermal behavior study of discharging/charging cylindrical lithium-ion battery module cooled by channeled liquid flow. *International journal of heat and mass transfer*, 120:751–762, 2018.

[40] Jiateng Zhao, Zhonghao Rao, and Yimin Li. Thermal performance of mini-channel liquid cooled cylinder based battery thermal management for cylindrical lithium-ion power battery. *Energy conversion and management*, 103:157–165, 2015.

[41] Zhiguo Tang, Xiaoteng Min, Anqi Song, and Jianping Cheng. Thermal management of a cylindrical lithium-ion battery module using a multichannel wavy tube. *Journal of Energy Engineering*, 145(1):04018072, 2019.

[42] Kreisel electric - battery technology pioneer. https://www.kreiselelectric.com/, 2023. Accessed: 2023-09-12.

[43] Said Al Hallaj and JR Selman. A novel thermal management system for electric vehicle batteries using phase-change material. *Journal of the Electrochemical Society*, 147(9):3231, 2000.

[44] Adil Wazeer, Apurba Das, Chamil Abeykoon, Arijit Sinha, and Amit Karmakar. Phase change materials for battery thermal management of electric and hybrid vehicles: A review. *Energy Nexus*, page 100131, 2022.

[45] Huaqiang Liu, Zhongbao Wei, Weidong He, and Jiyun Zhao. Thermal issues about li-ion batteries and recent progress in battery thermal management systems: A review. *Energy conversion and management*, 150:304–330, 2017.

[46] Missing title. https://www.pistonudos.com/en/electricity-on-board-from-the-alternator-to-the-electric-car-ii, 2023. Accessed: 2023-09-12.

[47] Tedjani Mesbahi, Rocío Bendala Sugrañes, Reda Bakri, and Patrick Bartholomeüs. Coupled electro-thermal modeling of lithium-ion batteries for electric vehicle application. *Journal of Energy Storage*, 35:102260, 2021.

[48] Hamidreza Behi, Danial Karimi, Mohammadreza Behi, Morteza Ghanbarpour, Joris Jaguemont, Mohsen Akbarzadeh Sokkeh, Foad Heidari Gandoman, Maitane Berecibar, and Joeri Van Mierlo. A new concept of thermal management system in li-ion battery using air cooling and heat pipe for electric vehicles. *Applied Thermal Engineering*, 174:115280, 2020.

7 Appendix

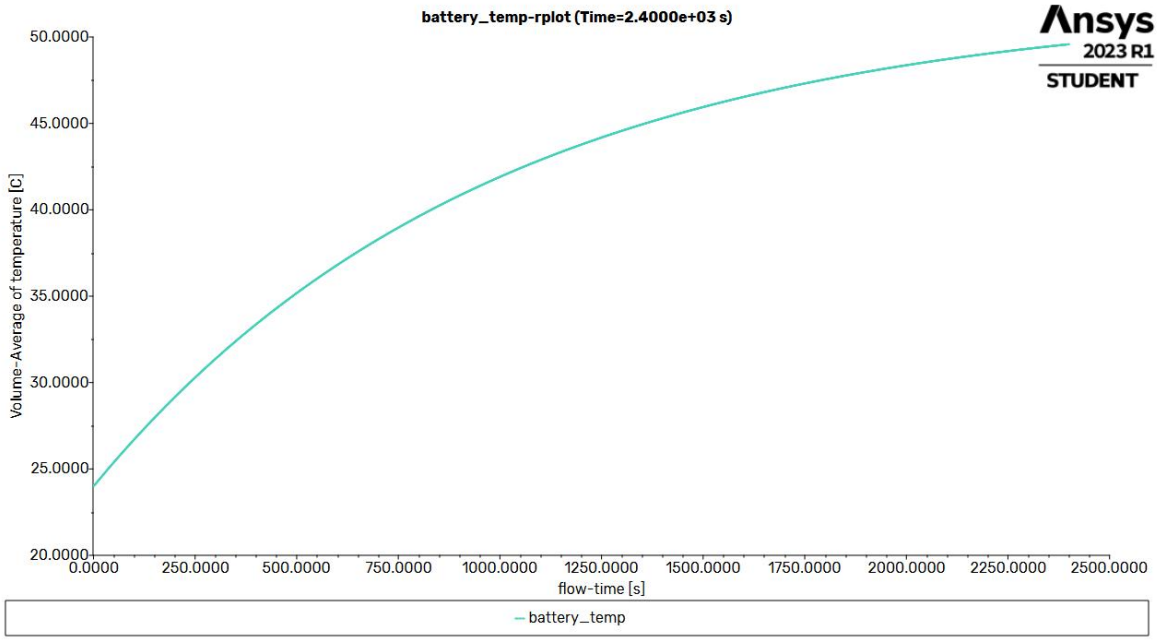

Figure 46: Average temperature plot of 1.5C at 0.5 m/s

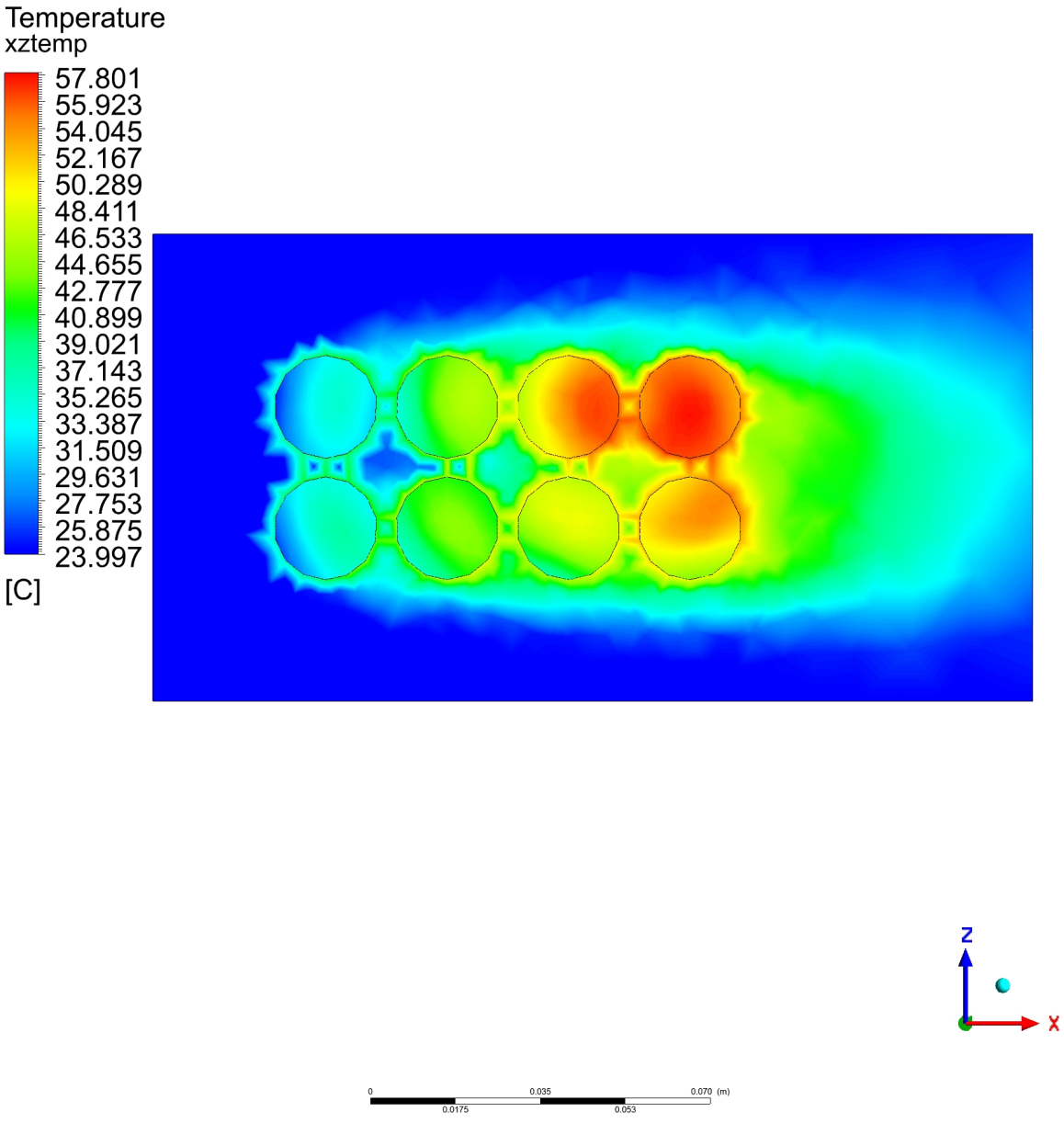

Figure 47: Temperature contour of 1.5C at 0.5 m/s

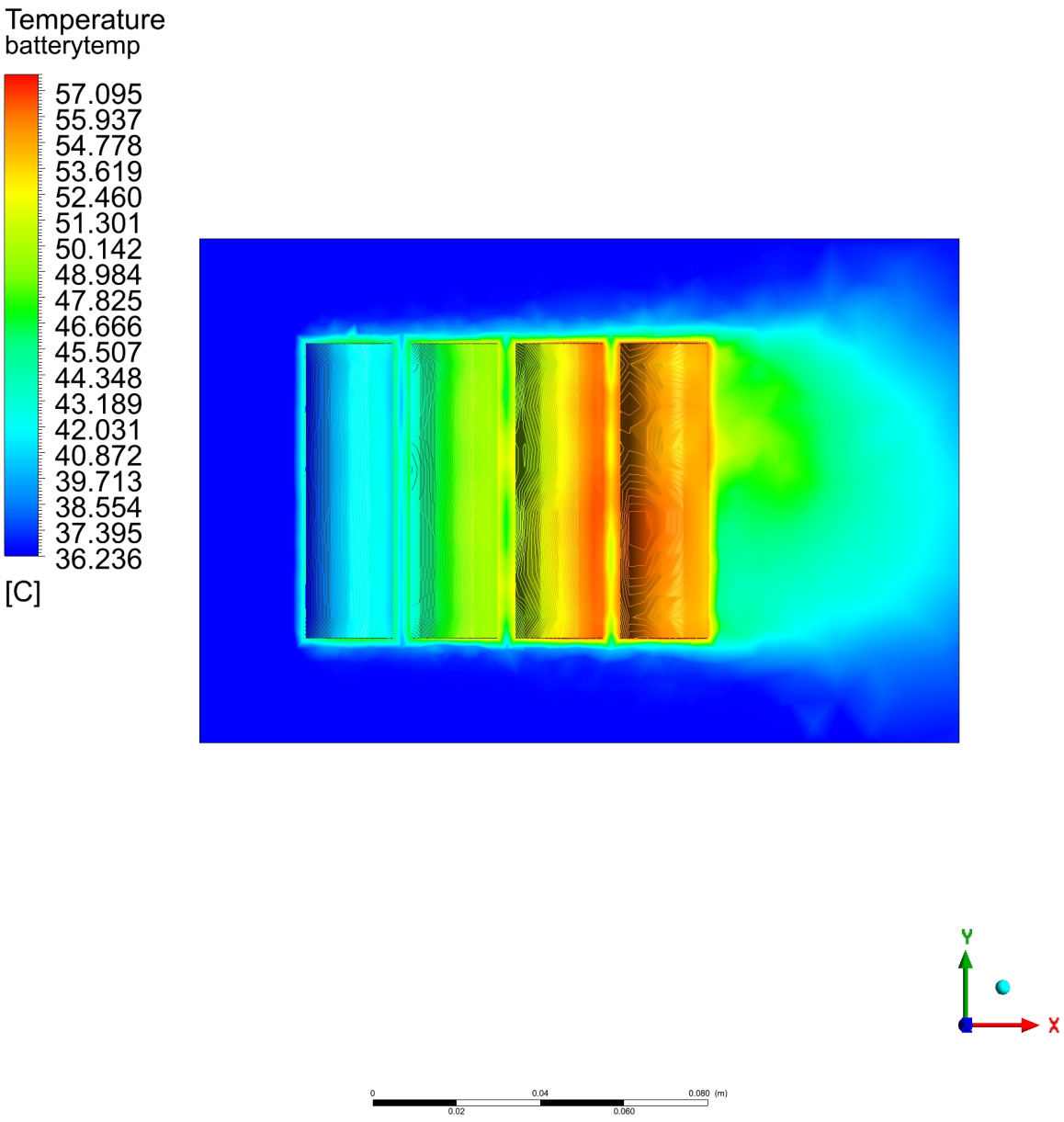

Figure 48: Temperature contour of 1.5C at 0.5 m/s

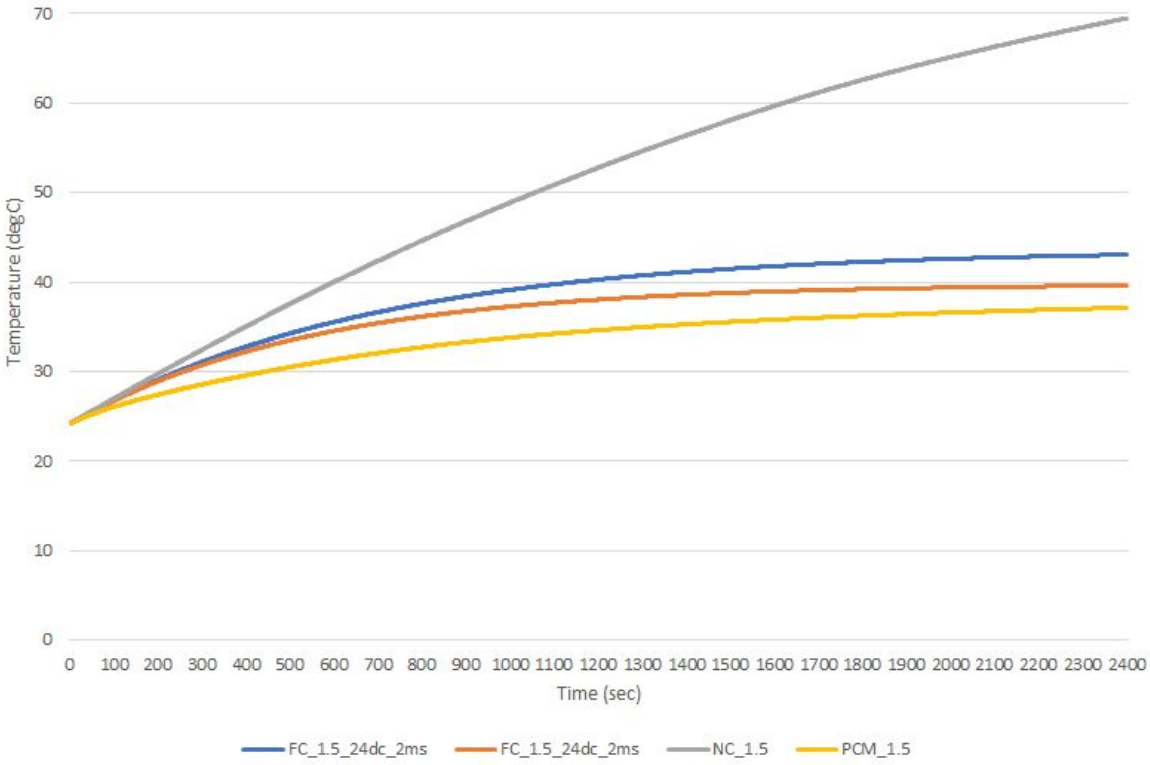

Figure 49: Avg. Temperature variation different cooling methods

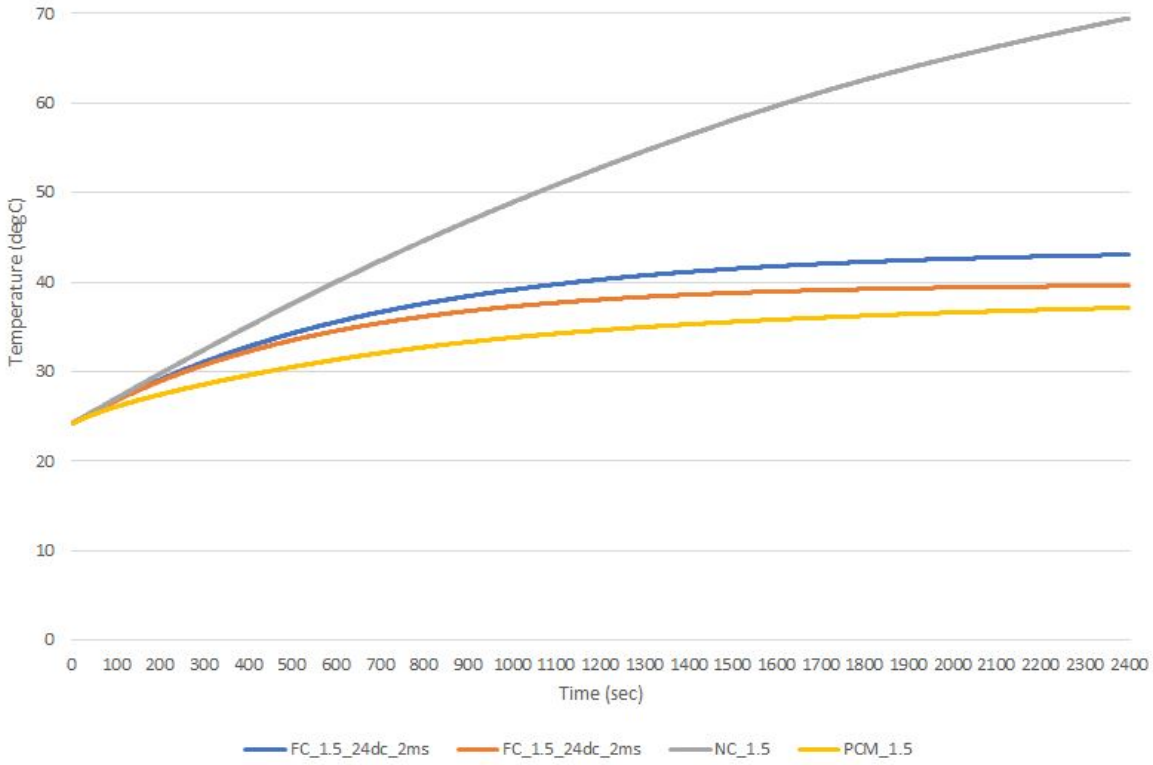

Figure 50: Avg. Temperature variation different cooling methods

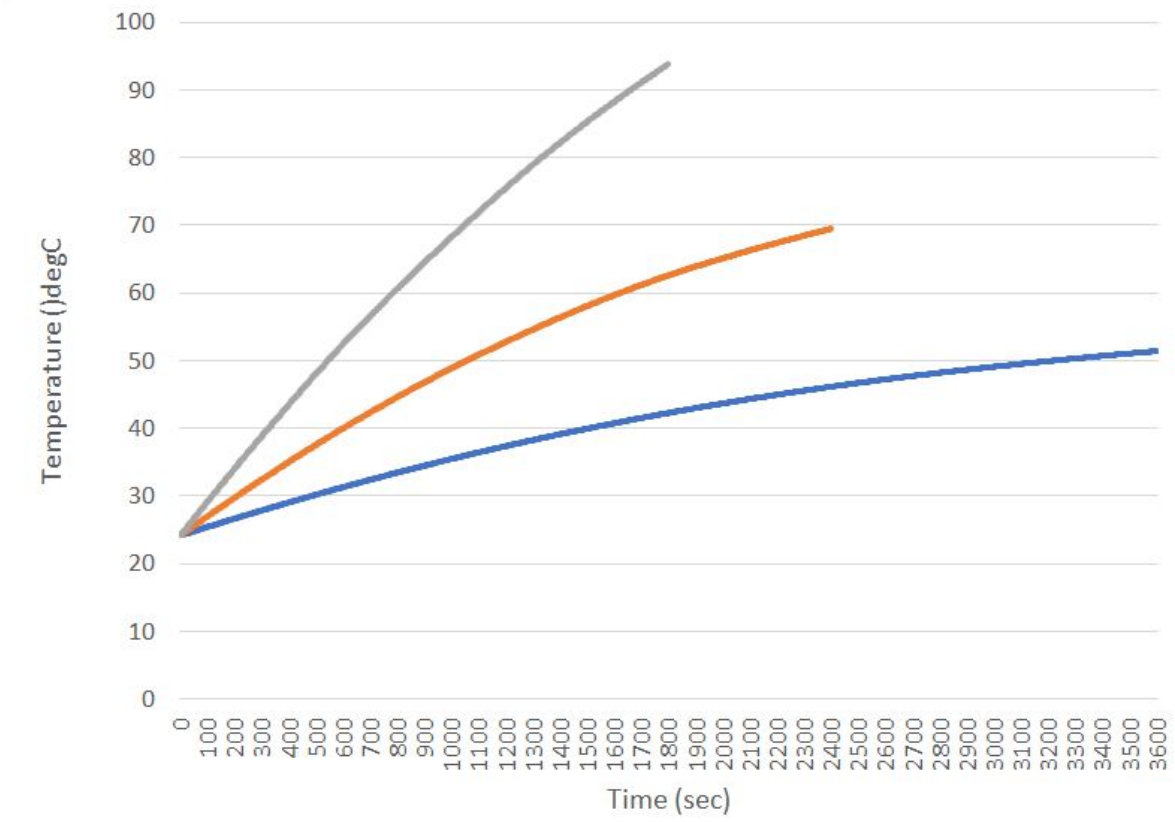

Figure 51: Natural convection at a constant temperature different C-Rates 2mm spacing

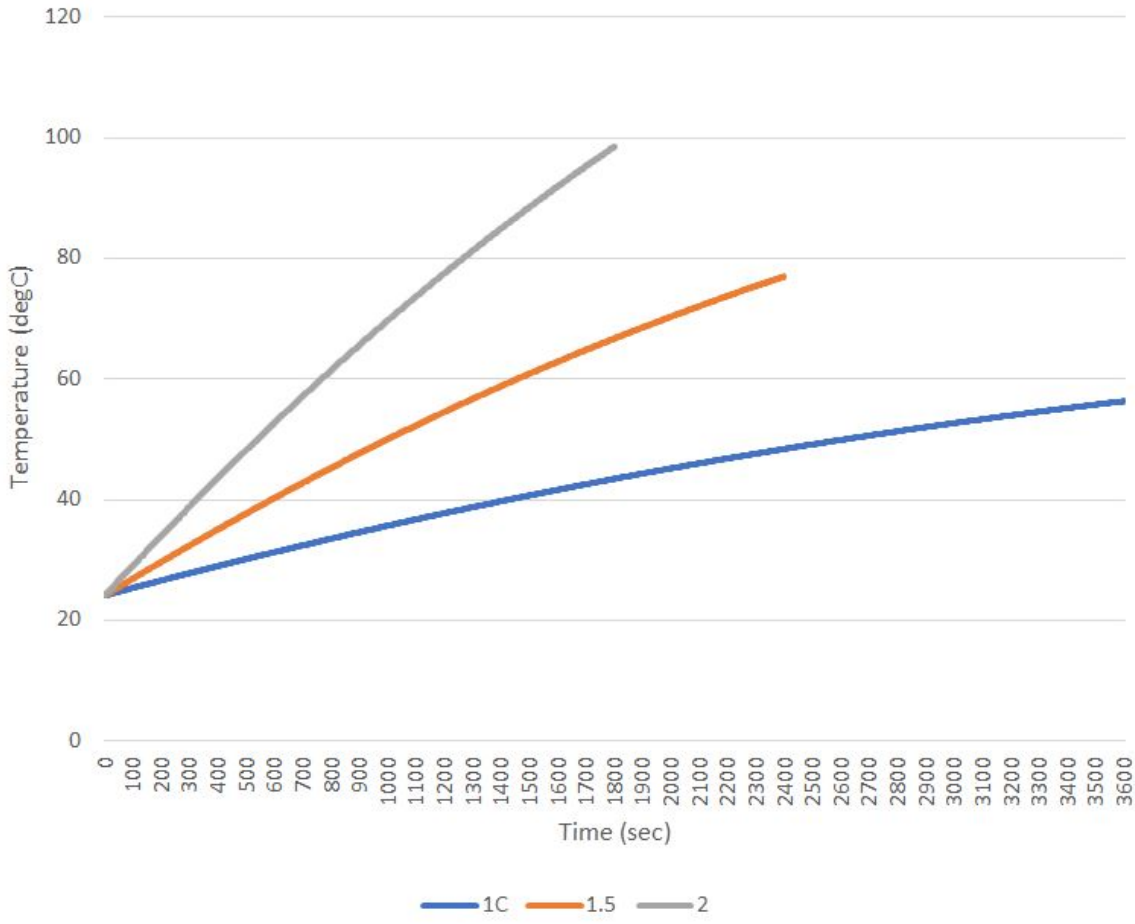

Figure 52: Natural convection at a constant temperature different C-Rates 4mm spacing

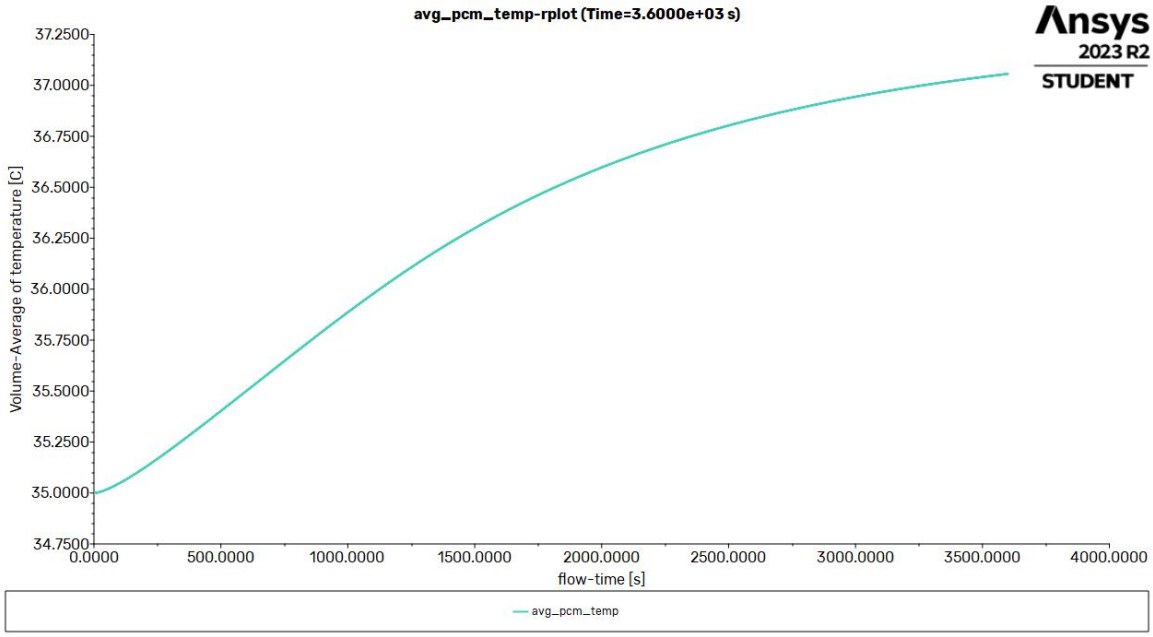

Figure 53: Average PCM temperature for 35degC at 4mm spacing

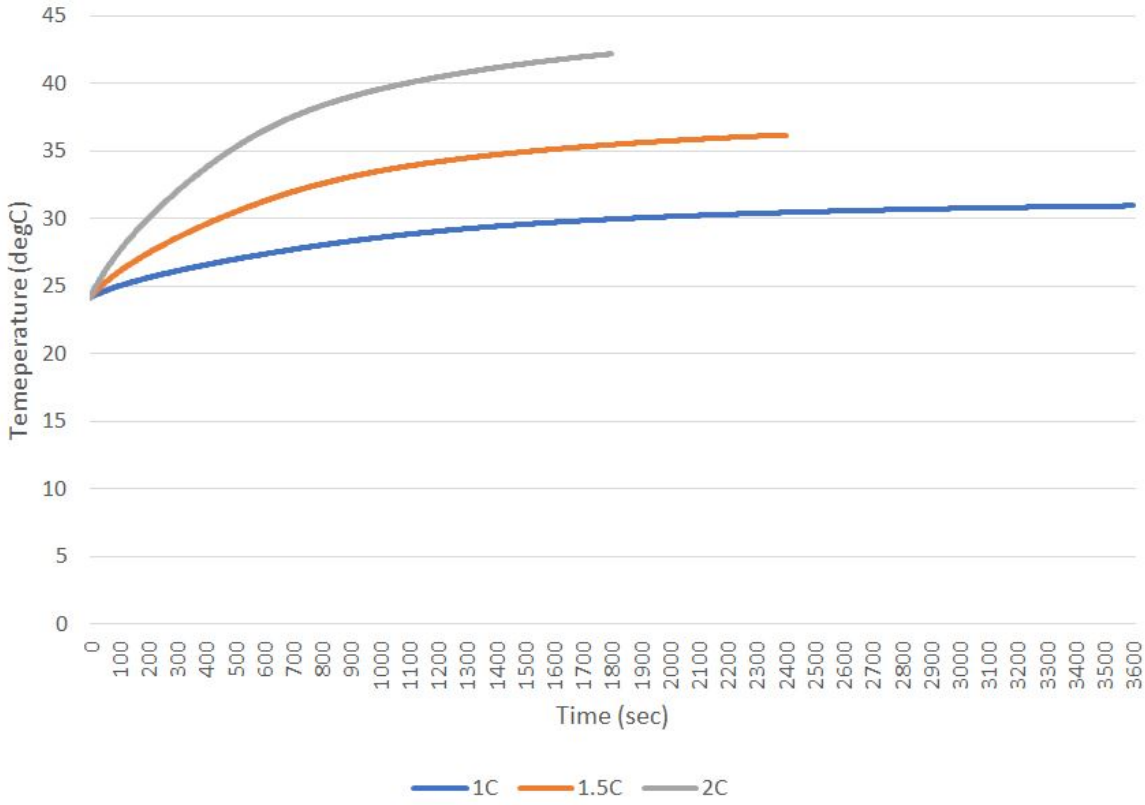

Figure 54: PCM temperatures at different C-rates

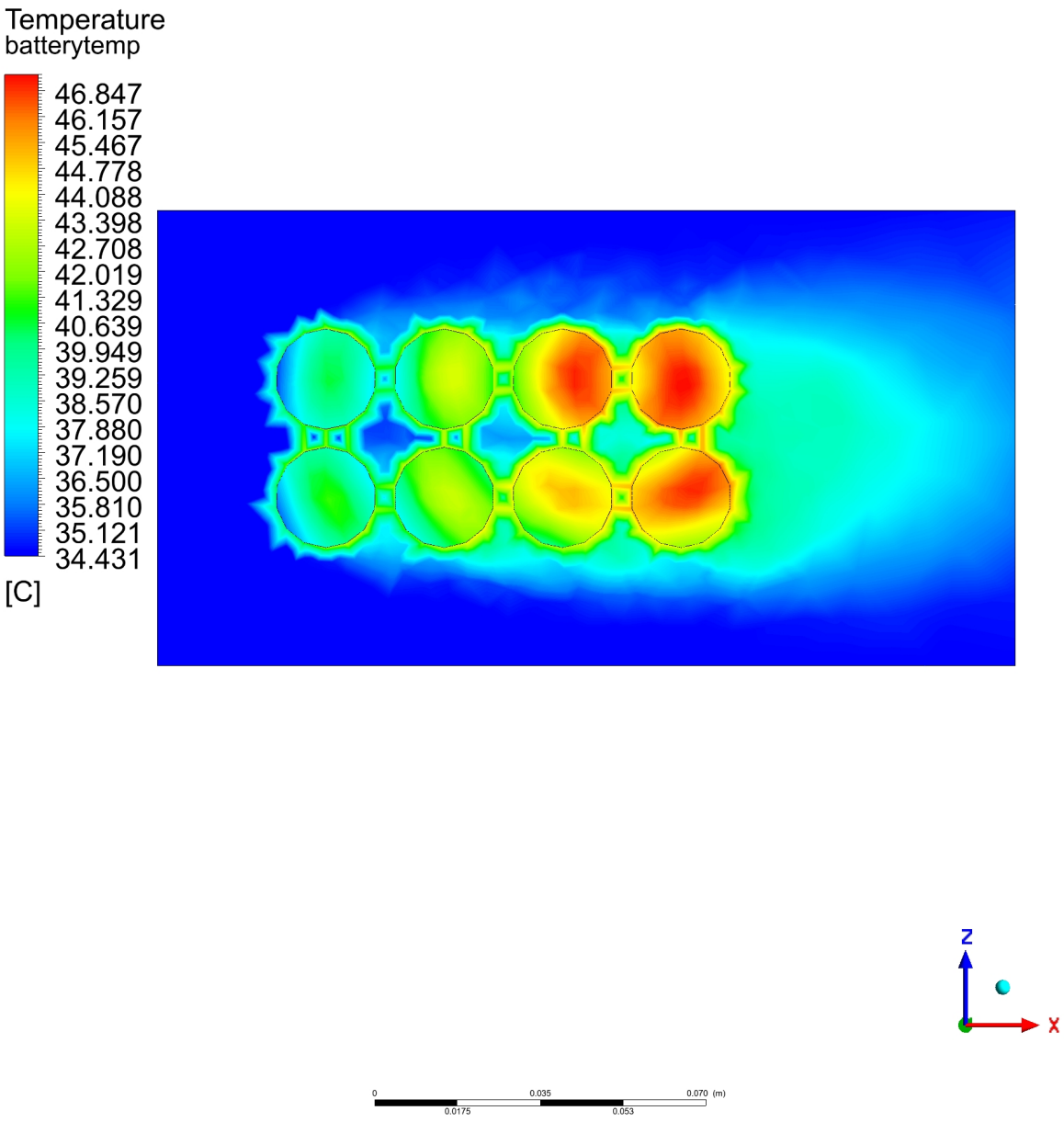

Figure 55: Top view 1.5C 1m/s

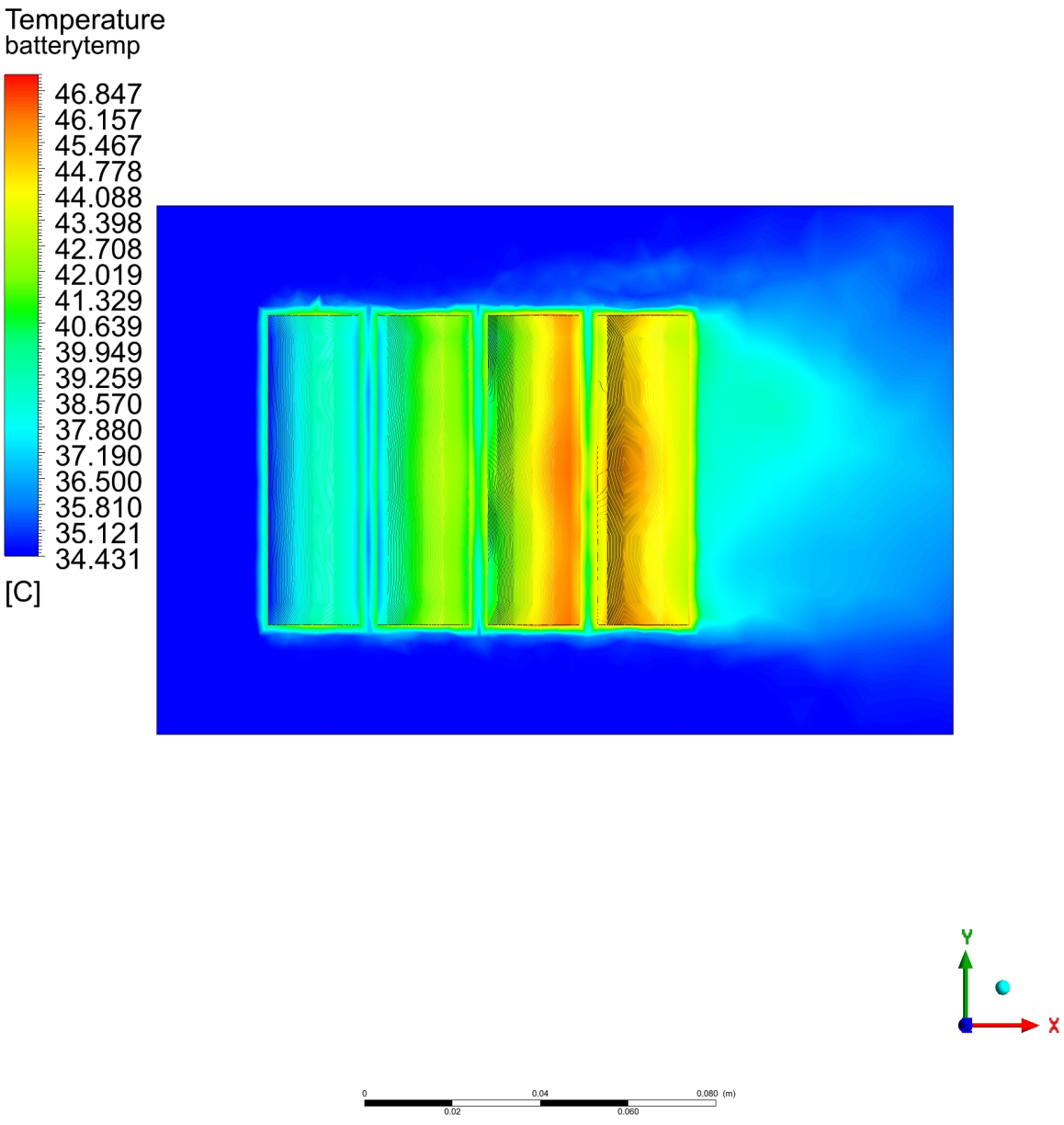

Figure 56: Side view 1.5C 1m/s

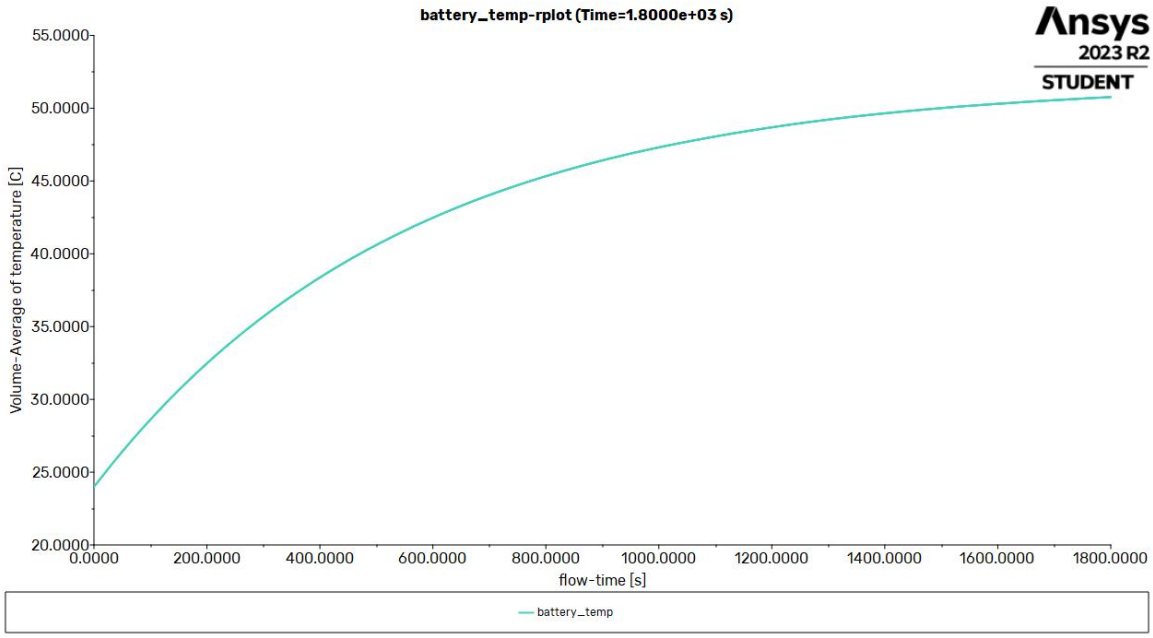

Figure 57: Average battery tempearture 2C 2m/s

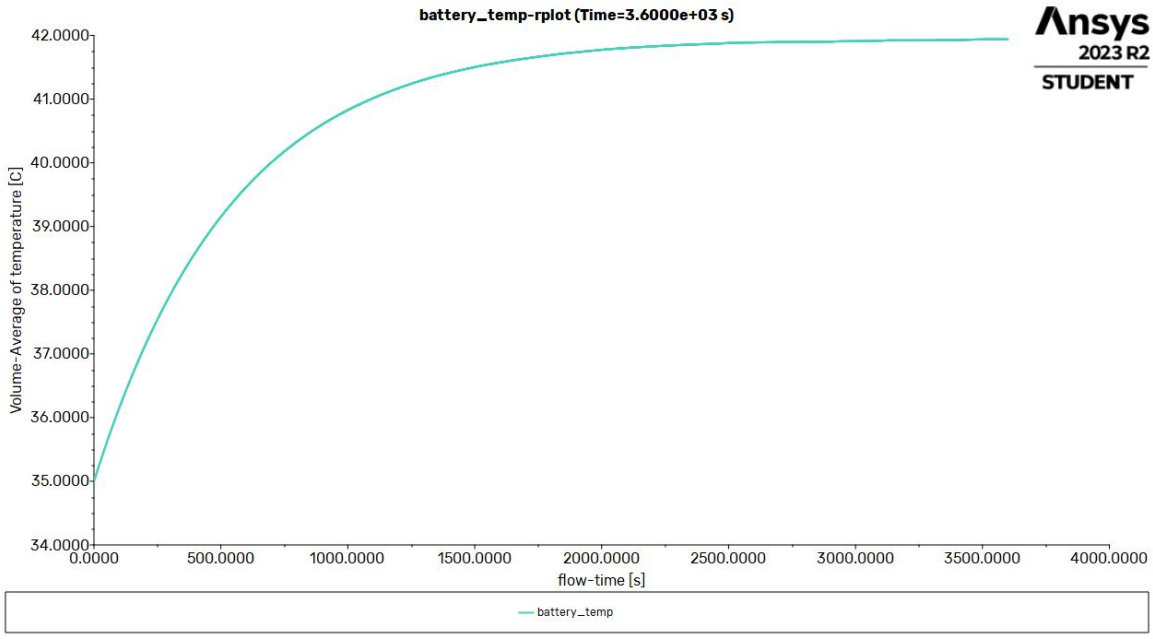

Figure 58: Average battery tempearture 1C 2m/s